

1 **Developing luminescence analysis of Icelandic volcanic glass: a case study**  
2 **using the Þórsmörk Ignimbrite**

3

4 Stephen J. Roberts<sup>1, \*</sup>, David C.W. Sanderson<sup>2</sup>, Andrew J. Dugmore<sup>3</sup>

5

6 <sup>1</sup> British Antarctic Survey (BAS), Natural Environment Research Council (NERC), High Cross,  
7 Madingley Rd, Cambridge, CB3 0ET, UK.

8 <sup>2</sup> SUERC, Scottish Enterprise Technology Park, Rankine Avenue, East Kilbride, Glasgow G75  
9 OQF, Scotland.

10 <sup>3</sup> School of GeoSciences, University of Edinburgh, Drummond Street, Edinburgh EH8 9XP.

11

12 **\*Corresponding author:**

13 e-mail: [sjro@bas.ac.uk](mailto:sjro@bas.ac.uk), Tel: +44 (0)1223 221 339; Fax: +44 (0)1223 221 259

14 Twitte: @roberts\_sjr

15 This paper is a non-peer reviewed preprint submitted to EarthArXiv

16

17 **Keywords:** Tephra; geochronology; geochemistry; Arctic; palaeoclimate

18 **Abstract**

19 Large volcanic eruptions from Iceland can produce significant volumes of glass-rich rhyolitic  
20 tephra, which are then deposited across NW Europe and the North Atlantic-Arctic region,  
21 forming time-parallel marker horizons useful to palaeoenvironmental studies. Here we  
22 investigate new ways of improving the tephrochronological record of Iceland using  
23 (thermo)luminescence analysis of rhyolitic volcanic glass shards that dominate airfall ash  
24 deposits of the Þórsmörk Ignimbrite (ÞIG), tephra from the Askja 1875 AD, Öræfi 1362 AD  
25 eruptions, and the Óþoli tephra from NW Iceland. Following screening experiments, which  
26 showed that pure volcanic glass samples retained age-related TL signals, we undertook glass-  
27 phase TL dating of the ÞIG and Óþoli tephra. Our TL age estimate of  $c. 40 \pm 10$  ka for the ÞIG  
28 supports phenocryst-based radiometric ages of  $c. 50$  ka rather than older age estimates of  $c.$   
29  $200$  ka. Results from the Óþoli tephra were consistent with the fission track age established  
30 at  $c. 2$  Ma age, but further investigations of high dose sensitivity changes and longer-term  
31 stability factors such as athermal fading are required for quantitative dating of volcanic glass  
32 deposits  $>100$  ka. However, as thermoluminescence signals from purified glass fractions of  
33 Icelandic tephra can be obtained over 100–1,000,000-year time scales, luminescence  
34 characterisation of glass shards can be used alongside geochemical and morphological  
35 analysis to distinguish between distal tephras with similar geochemical signatures, and assist  
36 with tephrochronological investigations beyond the limits of radiocarbon dating.

37

38

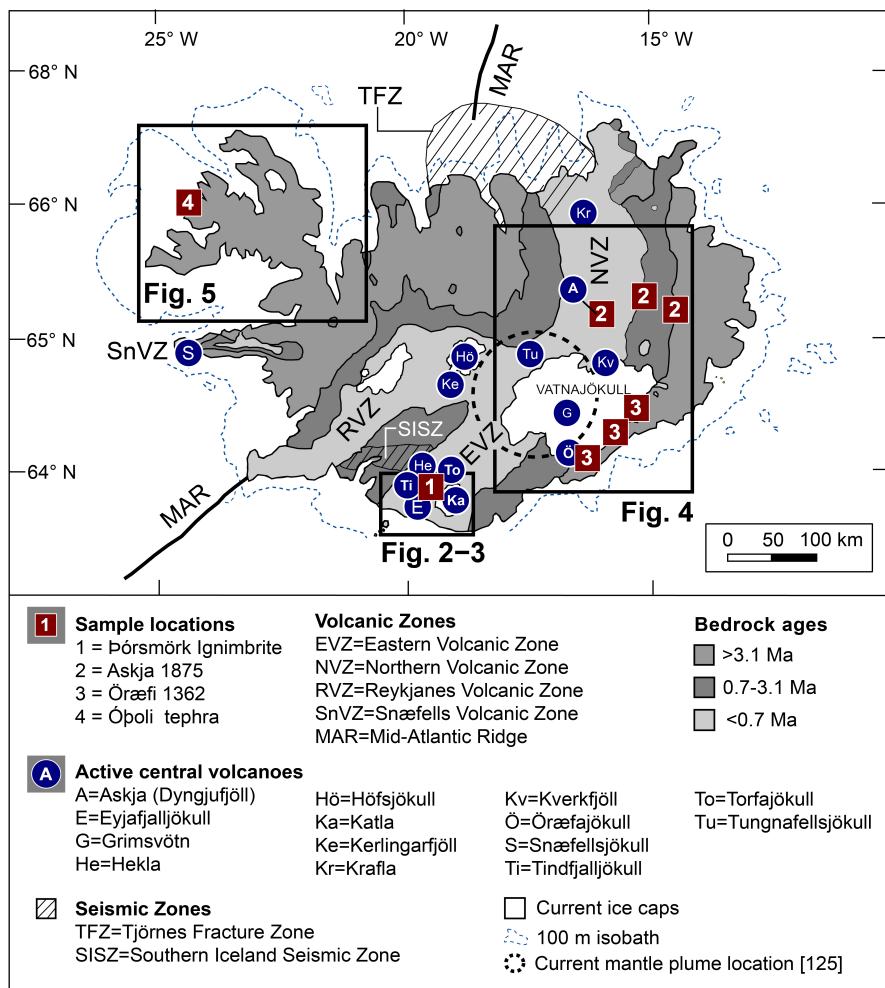
## 39 Introduction

40 Large explosive rhyolite-producing eruptions from Iceland, such as the one responsible for  
41 the Þórsmörk Ignimbrite (PIG) in southern Iceland (Fig. 1), are comparatively rare, but  
42 particularly useful as they form time-parallel marker horizon, which provide chronological  
43 constraints for palaeoenvironmental records. As recent eruptions from Iceland have shown,  
44 volcanic ash from even comparatively small eruptions can be distributed across the North  
45 Atlantic and Arctic regions, and north-western Europe. Numerous studies have used of tephra  
46 layers to link ice, marine and terrestrial records of past environmental and climate change  
47 [1–30], but glacial erosion has removed many of the largest eruptions of the pre-Holocene,  
48 Quaternary era (>11.7 ka–2.5 Ma) from the Icelandic terrestrial record and some key large  
49 Pleistocene eruptions remain relatively poorly characterised and dated near their sources.

50

51 To be useful as time-parallel marker horizons, tephra deposits need to be fully characterised.  
52 Major and trace element geochemistry and phenocrystic composition are commonly used  
53 alongside shard morphology, texture and chronological data to distinguish between different  
54 tephra deposits, and correlate those that are similar [24, 27–42]. However, geochemical  
55 correlation based on glass major element geochemistry can sometimes be problematic.  
56 Multiple eruptions from the same magma body can produce geochemical heterogeneity  
57 within the glassy products of individual deposits [43, 44], but different eruptions from the  
58 same magma chamber over a period of time can also produce glass with broadly similar major  
59 element geochemical composition. Recent studies have shown there are significantly more  
60 visible and non-visible (crypto-tephra) Icelandic ash deposits in sediment cores extracted  
61 from the Arctic Sea and North Atlantic than previously thought, and not all can be  
62 distinguished by shard-specific major or trace element analysis [33, 37]. Widely dispersed

63 tephra deposits can also be re-deposited a long time after the eruption event by post eruption  
 64 processes such as ice-rafting [45, 46] and several studies have confirmed that glass is not  
 65 geochemically stable in all burial environments or able to withstand harsh laboratory  
 66 digestion procedures intact [47, 48].



67  
 68 **Figure 1.** Summary geological map of Iceland showing active central volcanoes and sample  
 69 locations [adapted from 11].

70  
 71 More than 300 historical eruptions have been documented or identified by geochemical  
 72 analysis of tephra layers in Iceland in the last c. 1,100 years, on average, one every four years  
 73 [7, 10, 11, 29, 49-59]. Tephra is the only product of more than 130 of these eruptions, and

74 over 75 % of these have produced a visible tephra layer on the Icelandic mainland [60].  
75 However, rhyolitic tephra and large ignimbrite-forming eruptions are relatively uncommon in  
76 the Icelandic tephrochronological record [13, 15, 37, 53, 61].

77

78 Since rhyolitic magmas produce the most geochemically evolved and distinctive tephra,  
79 geochemical discrimination between different volcanic systems and/or multiple eruption  
80 events from the same volcanic system can be achieved. Moreover, large volumes of rhyolitic  
81 volcanic glass, which are unequivocally associated with the eruption event, form explosively  
82 on contact with water and/or ice during magma-quenching. For example, volcanic glass  
83 formed from the rhyolitic magma of the Öräfi 1362 AD eruption is geochemically  
84 homogenous and has <1% phenocrystic content [62]. Glass-rich volcanic ash ejected into the  
85 stratosphere can be distributed over a wide geographical area, forming long-distance  
86 chronological markers [63, 64]. Advantageously, selective removal of heavier phenocrystic  
87 components during long-distance stratospheric transport of ash provides a natural glass-  
88 purification process.

89

90 Radiation induced thermoluminescence (TL) is a well-established property of crystalline  
91 minerals such as quartz and feldspars [65]. Non-crystalline materials including synthetic glass  
92 [66,67] and naturally occurring volcanic glass (*e.g.*, obsidian) [68] also exhibit TL, though with  
93 lower sensitivities than most crystalline materials. A study of 55 archaeological silicate glass  
94 slices [66] showed high temperature TL sensitivities ranging from  $10^{-1}$  to  $10^2$  photon counts  
95 per mg per Gy in 10 degree centigrade bands. By contrast TL sensitivities from quartz samples  
96 from diverse lithologies have been reported [111] as ranging from  $10^3$ - $2 \times 10^4$  photon counts

97 per mg per Gy over similar temperature intervals (centred on 380 degrees centigrade), and  
98 from feldspars from  $10^4$ - $10^6$  photon counts per mg per Gy.

99

100 Therefore, though volcanic glass is a metastable material [72], luminescence signals from the  
101 glass phase of tephra provide a useful additional provenance and, potentially, chronological  
102 tool, especially in the c. 50-75 ka age-range, which is difficult to date radiometrically in the  
103 absence of suitable phenocrysts [68–70]. Despite the relatively low signal levels, and  
104 variability in signal outputs due to retention of some fine crystalline components, pioneering  
105 luminescence studies from the early 1980s on fine-grained volcanic glass-rich fractions from  
106 tephra deposits from North America and New Zealand showed considerable potential [73–  
107 74].

108

109 Here, first, we investigate new ways of improving the tephrochronological record of Iceland  
110 by characterising the geochemical and TL properties of the (airfall) rhyolitic glass component  
111 that dominates tephra (>95%) from four key rhyolitic Icelandic eruptions of Late Quaternary  
112 age: the Þórsmörk Ignimbrite (ÞIG), the Ópoli tephra (ÓT), the Askja 1875 AD (A1875) and  
113 Öräfi 1362 AD (Ö1362) eruptions and (Figs. 1–6; Supplementary Fig. S1, Table S1). Second,  
114 we focus on producing quantitative ages from the ÞIG and compare our results to published  
115 age estimates.

116

117 Based on geochemical correlation to potassium-argon dated phenocrysts from ignimbrite  
118 deposits outside of the Þórsmörk area [1, 2], the ÞIG was originally considered to be c. 200  
119 ka. An argon-argon (Ar-Ar) age of  $54.5 \pm 2$  ka [3] has been geochemically linked to the c. 55 ka  
120 North Atlantic Ash Zone-II (NAAZ-II) II-RHY-II deposit, a widespread and geochemically

121 homogenous tephra deposit found in North Atlantic and Arctic Sea marine sediment cores  
122 Greenland ice core records [3–5]. The eruption that formed the ÞIG is the same order of  
123 magnitude as the thickest rhyolitic tephra layers in the Holocene and historical  
124 tephrochronological record of Iceland, *e.g.*, Hekla 3, Hekla 4, Öræfi 1362 AD and Askja 1875  
125 AD [11, 76, 88, 89].

126

127 The Óþoli tephra was found in plateau-top ice-dammed lake deposits of NW Iceland.  
128 Following initial TL analysis which suggested an early Quaternary age and has been fission-  
129 track dated to  $2.26 \pm 0.11$  Ma [75]. In this study, the tephra deposit acts as an ‘older’ age-  
130 comparison for quantitative TL dating of purified volcanic glass from the ÞIG.

131

132 The A1875 and Ö1362 tephra deposits examined are from two of the largest rhyolite forming  
133 Plinian eruptions in the Icelandic historical record. These eruptions distributed large volumes  
134 of tephra across eastern Iceland and NW Europe. In this study, we use them as ‘recent’ TL  
135 age-controls because they have similar glass-phase rhyolitic geochemistry to the Óþoli tephra  
136 and the ÞIG.

137

### 138 **Study sites**

139

140 **Þórsmörk Ignimbrite:** The Þórsmörk Ignimbrite (ÞIG), first described by Thórarinsson [1] and  
141 named by Jørgensen [76, 77], is located in the transitional-alkalic province of the Eastern  
142 Volcanic Zone (Fig. 1). It is one of Iceland’s largest eruptive bodies, covering an area of about  
143  $80 \text{ km}^2$  (Figs. 2, 3). Outcrops in the Þórsmörk area are the only known record of the ÞIG-  
144 forming eruption in the Icelandic terrestrial tephra record. Intermittent volcanic aggradation

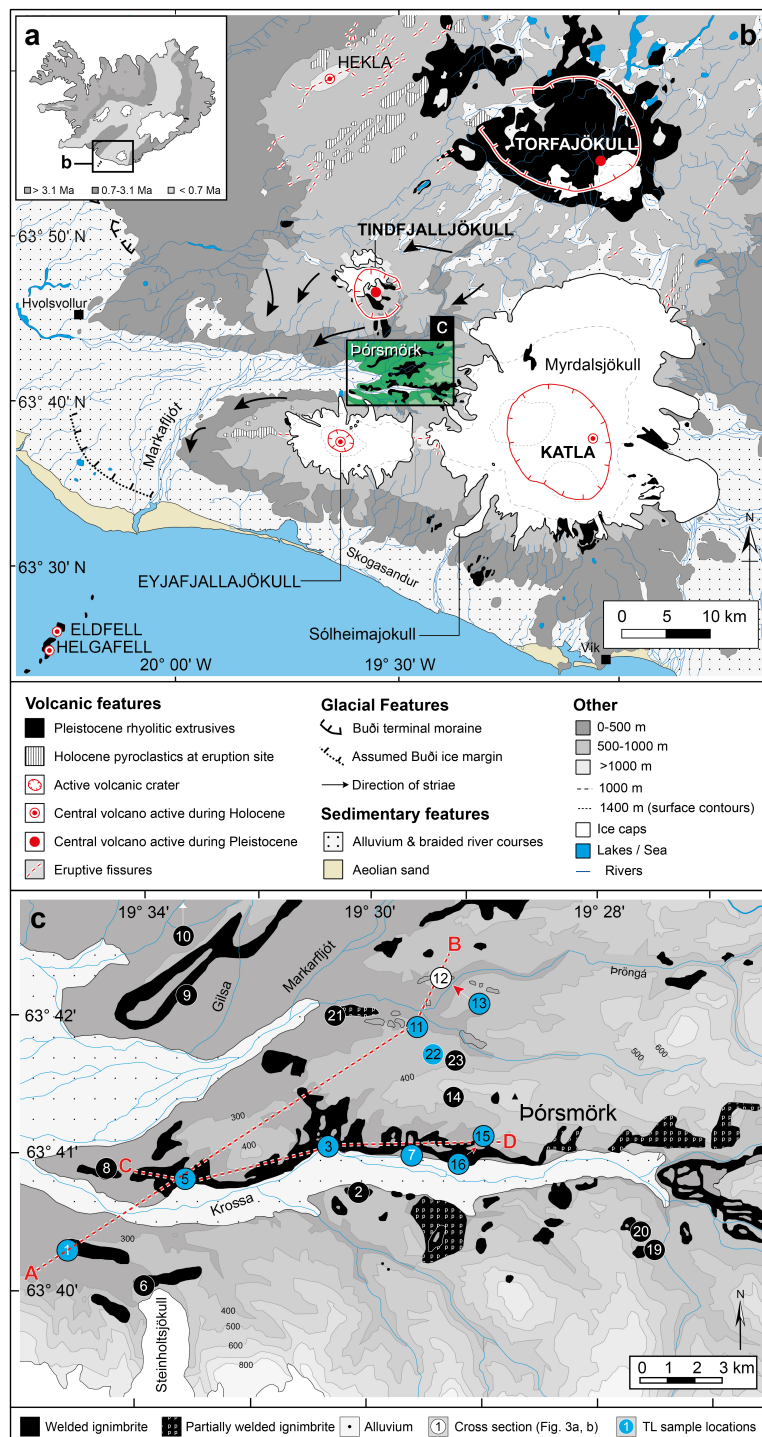
145 and glacial erosion have exposed well-preserved stratigraphic sections along the Krossa and  
146 Markarfljót valleys, with deposits north of the Krossa that are typically 10–50 m thick but can  
147 be up to 200 m thick [76, 77] (Figs. 2, 3). Accessible exposures, up to 30 m thick, are located  
148 on a 4–5 km stretch along the northern border of the Krossa (Figs. 2, 3). No basal contact is  
149 visible at most sites and only slope deposits are accessible at some sites [1, 76] (Fig. 3).

150

151 The Þórsmörk area is surrounded by three ice-capped, active central volcanoes: Eyjafjalljökull  
152 to the south, Katla to the east, Tindfjalljökull to the north (Fig. 2b). Torfajökull, Iceland's  
153 largest active rhyolite volcano, is located further to the NE and Hekla is located further north  
154 beyond Tindfjalljökull. Torfajökull is amongst the most active rhyolitic volcanoes in the world  
155 with at least ten rhyolitic eruptions in the post-glacial period alone with the last occurring in  
156 ca. 1480 AD [78]. Tindfjalljökull is the least active central volcano in this region and classified  
157 as a dormant volcano because there have only been a few eruptions along its margins in post-  
158 glacial times [1, 79, 80]. Eruptions from Tindfjalljökull are typically dominated by slightly  
159 alkaline basalts and minor intermediate rocks and abundant sub-alkaline to slightly  
160 peralkaline rhyolites [76, 80–83]. Thórarinsson suggested that the summit of Tindfjalljökull is  
161 collapse caldera connected with the formation of the ÞIG [1, 76, 84]. All structural and  
162 depositional features of the ÞIG preserved in and around Þórsmörk are associated with  
163 emplacement from pyroclastic flows or surges [76, 77] (Fig. 3). Jørgensen [76, 77] found no  
164 evidence for a Plinian phase of activity, but abundant airfall ash deposits (*e.g.*, Fig. 3i–l) could  
165 have been formed by explosively-generated pyroclastic flows, created by instabilities in the  
166 lower parts of the eruption column [85]. These combined into an ignimbrite-forming surge  
167 that mantled the existing topography, with welded and unwelded pumice and ash forced into  
168 valley troughs and sides. Given an average thickness of 20–25 m, Thórarinsson [1] calculated



169 that the equivalent volume of the BIG as 1.5–2.0 km<sup>3</sup>. At least a further 2–3 km<sup>3</sup> of freshly  
 170 fallen tephra was probably dispersed over a wider area, but this has since been eroded by  
 171 glacial activity.

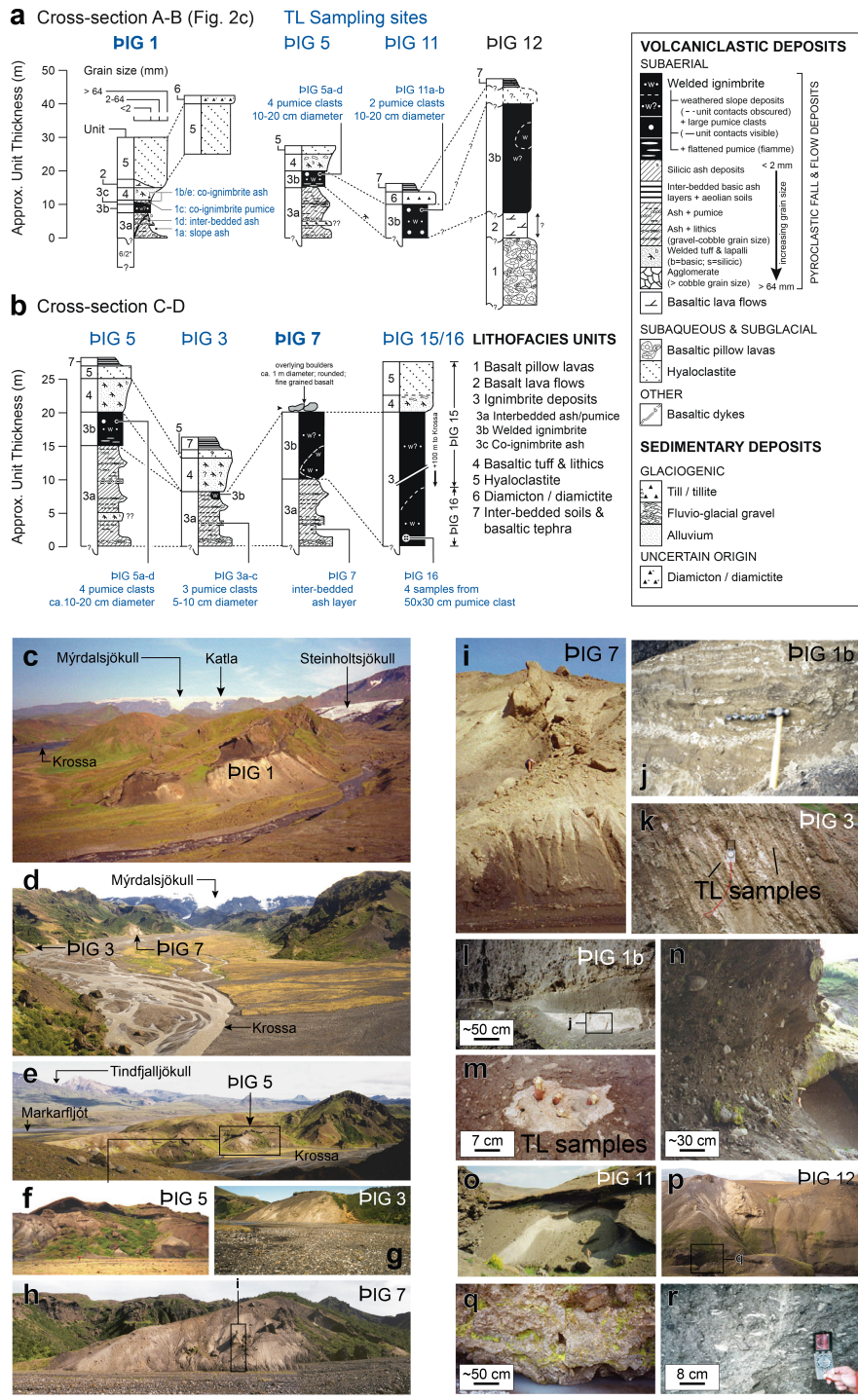


172  
 173 **Figure 2. Regional setting and sampling locations for the Þórsmörk Ignimbrite. (a)** Location  
 174 **map of Iceland; (b)** Location map of Þórsmörk in relation to active volcanoes, pyroclastic and

175 extrusive deposits and main glacial features of the Eastern Volcanic Zone (EVZ), Iceland. The  
176 geology of area covered by the Þórsmörk box is basic and intermediate hyaloclastites and  
177 tuffaceous sediment younger than 0.7 Ma (based on the 1:250,000 Geological Map no. 6 of  
178 the Iceland Geodetic Survey). **(c)** Sketch map of main outcrops of the Þórsmörk Ignimbrite,  
179 and its broad classification into welded and unwelded outcrops [adapted from 76, 77] and  
180 thermoluminescence sampling locations (blue circles) investigated in this study. Some sample  
181 sites (*e.g.*, ÞIG10) were located off-map, while others (*e.g.*, ÞIG12) were inaccessible.

182

183 Thórarinnsson [1] and Jørgensen [77] both suggested a c. 200 ka age for the ÞIG by correlating  
184 deposits in Þórsmörk with potassium-argon (K-Ar) ages from geochemically similar deposits  
185 north of Þórsmörk [2, 4]. Zielinski et al. [9] later proposed that the ÞIG was the source of the  
186 rhyolitic component of North Atlantic Ash Zone-II (NAAZ-II), a widespread tephra deposit that  
187 has been found in numerous marine and ice cores across the North Atlantic and the Arctic  
188 Sea (Fig. S1). Dated to c. 50 ka, based on its correlation-based age in the GISP2 Greenland ice  
189 core of 53.5-55 ka [9, 86, 87], NAAZII has been geochemically linked with an argon-argon (Ar-  
190 Ar) dated ÞIG deposit of  $54.5 \pm 2.0$  ka, sampled from an unspecified location [3].



191

192 **Figure 3. The Þórsmörk Ignimbrite, southern Iceland. (a–b) Summary composite schematic**

193 **stratigraphic logs of main lithofacies units at principal sites and schematic cross section**

194 **sketches along lines A-B and C-D; (c–r) Photographs of the Þórsmörk Ignimbrite sampling**

195 **locations and luminescence sampling methods: (c) Site PIG 1, taken from the lateral moraine**

196 **of Gigjökull, looking approximately E up the Krossa towards Myrdalsjökull; (d) Sites PIG 3 & 7,**

217 taken from Valahnjúkur looking approximately E up the Krossa towards Mýrdalsjökull; **(e)** Site  
218 PIG 5, taken from the top of site PIG 6, looking approximately NNE towards Tindfjalljökull in  
219 the distance; **(f)** Site PIG 5; **(g)** Site PIG 3 looking approximately W down the Krossa; **(h)** Site  
220 PIG 7 taken from the Krossa sandur looking N at sampling site, and erratics near the top of  
221 the deposit (circled); **(i)** TL sampling at site PIG 7 composed of inter-bedded ash, pumice and  
222 lithic layers beneath an outcrop of welded ignimbrite, similar to those at PIG 3, shown in (k);  
223 **(j)** TL sampling at PIG 1b in ash rich co-ignimbrite ash and pumice layers; **(k)** TL sampling of  
224 inter-bedded ash layers at PIG 3; **(l)** Co-ignimbrite ash, black tuff and capping hyaloclastites  
225 at site PIG 1b (Units 3c, 4, 5); **(m)** TL sampling of a large pumice clast, c. 25–30 cm in diameter,  
226 embedded in a welded ash and lithic matrix at site PIG 16; **(n)** Poorly sorted, rounded boulders  
227 and pebbles in loose soil and fine-grained matrix (diamicton) contact with welded ignimbrite  
228 at site PIG 11 (hammer for scale); **(o)** Site PIG 11 looking NNE (person at the bottom edge of  
229 the shadow for scale); **(p)** Site PIG 12 taken from the top of the hill at site PIG 13 looking  
230 approximately north; **(q)** Pillow lavas at the base of PIG 12; **(r)** Fiamme at the base of PIG 5  
231 (Unit 3b).

212

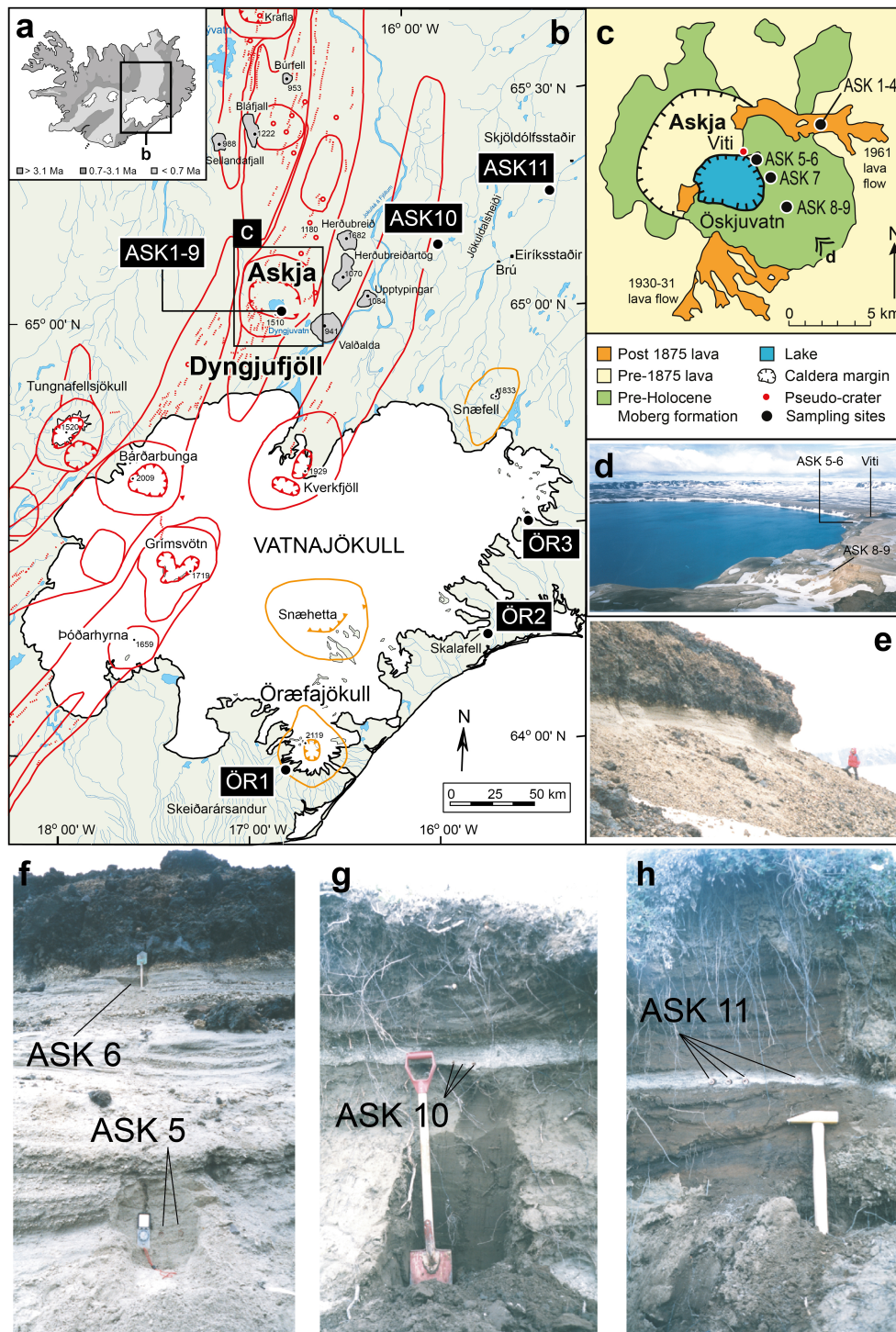
213 **Askja 1875 AD (A1875) tephra:** Post-glacial volcanism in Iceland is concentrated in four  
214 separate areas within the fissure system of Dyngjufjöll (Askja), located approximately 100 km  
215 North of Vatnajökull in the Eastern Highlands of the tholeiitic Northern Volcanic Zone (NVZ)  
216 of Iceland (Figs. 1, 4) [83]. Askja, the name of the main caldera and central volcano, covers an  
217 area of c. 45 km<sup>2</sup> (Fig. 4) and is bounded by steep cliffs, with Pleistocene-age rocks and  
218 predominantly basaltic composition forming the basement bedrock inside the crater (Fig. 4)  
219 [89]. Post-glacial lavas contain several rhyolitic ash layers, the oldest dated to c. 9,800 years  
220 BP [90]. Between 9,800-4,500 years BP, following rapid early Holocene deglaciation in Iceland,

221 volcanic productivity was 30 times greater than during the historical era [90]. The last Plinian  
222 eruption in the Dyngjufjöll volcano took place from within the Askja caldera a few hours  
223 before 8 a.m. on 29th March 1875 AD [90, 91]. The explosive phase of the eruption produced  
224 large volumes of fine-grained, grey-white, non-vesicular ash, which was dispersed across  
225 eastern Iceland by strong westerly winds forming visible layers 20-30 cm thick up to 50 km  
226 away [6]. The A1875 eruption is a classic example of how tephra from explosive Icelandic  
227 eruptions can be rapidly distributed across the North Atlantic and NW Europe [92, 93]. Tephra  
228 layers dominated by glass-shards invisible to the naked eye with a similar eruption-related  
229 geochemistry to A1875 deposits in Iceland have been found in Scandinavia [90, 94].

230

231 **Öræfi AD1362:** The Öræfajökull volcano, located in the Eastern Volcanic Zone on the southern  
232 margins of the Vatnajökull ice cap (Figs. 1, 4b), is Iceland's highest (2119 m) and most active  
233 composite stratovolcano during the post-glacial and Holocene era. There have only been two  
234 rhyolite-producing eruptions from Öræfajökull in the historical period: in 1362 AD and 1727  
235 AD [11]. The 1362 AD eruption (henceforth referred to as Ö1362) was particularly explosive,  
236 producing >10 km<sup>3</sup> of freshly fallen rhyolitic ash and pumice, and accompanied by two massive  
237 jökulhlaups from Falljökull and Rótarfjallsjökull. Although the eruption took place mainly in  
238 the caldera, and most of the fallout occurred over the sea, it is still the second most  
239 voluminous tephra deposit in Iceland in recorded history, after the more effusive and basaltic  
240 tephra producing Veiðivötn eruption of 1477 AD [58]. Up to 2 km<sup>3</sup> of highly evolved rhyolitic  
241 (SiO<sub>2</sub>>70%) tephra fell on land with prevailing westerly winds transporting most of the ejecta  
242 ESE across the North Atlantic [11, 62, 95]. Tephra layers up to 10 cm thick have been found in  
243 soils covering an area of 4300 km<sup>2</sup> surrounding the main edifice [96].

244



245

246 **Figure 4. Historical eruption age-control study sites and sampling of A1875 and Ö1362**

247 **tephra deposits. (a)** Location map; **(b)** Regional setting of the Askja (Dyngjufjöll) (red) and the

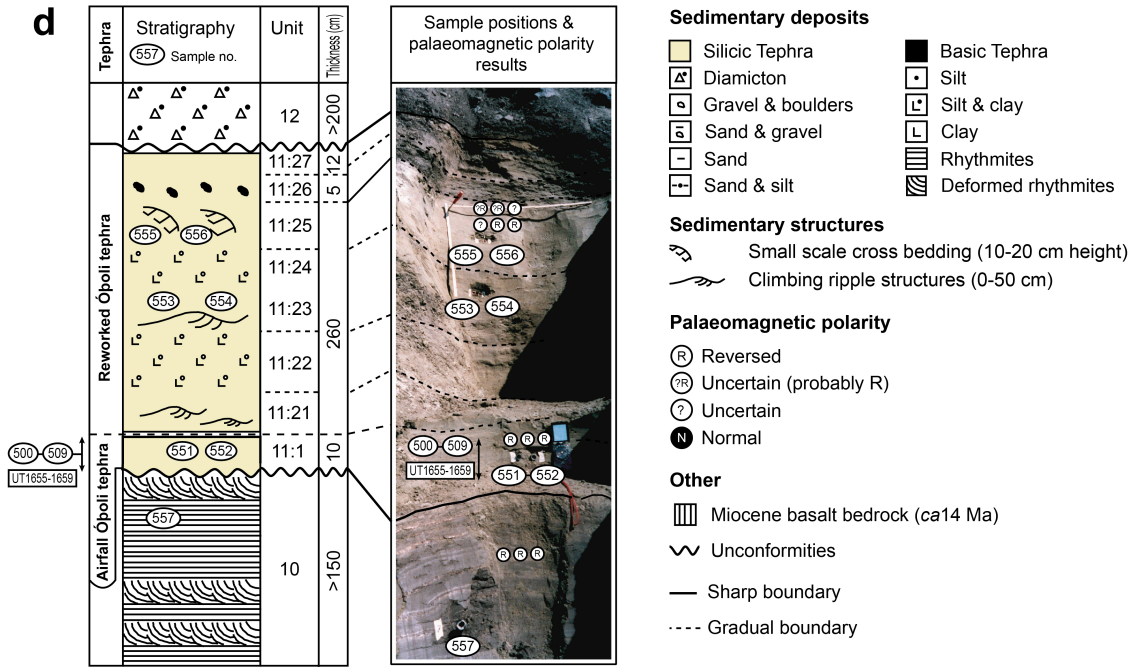
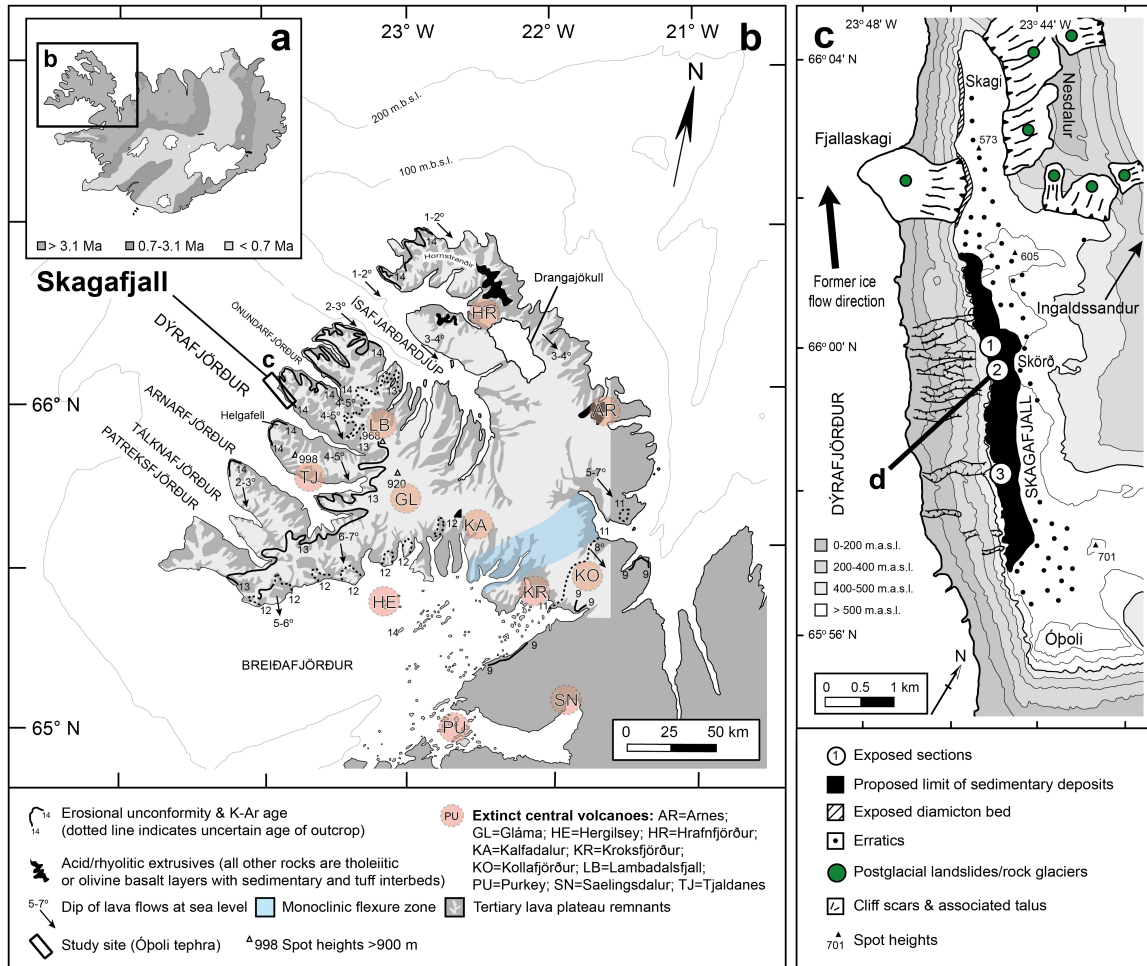
248 Öraefi (orange) volcanic systems and Askja 1875 (ASK1-11) and Öraefi 1362 (ÖR1-3) sampling

249 locations. Solid red & orange lines are outlines of the main volcanic systems; broken lines red

250 and orange lines are fissure swarms; triangulated lines are the caldera margin; red circles are

251 craters and grey areas outlines of the main table mountains ('mobergs'). **(c)** Summary  
252 geological map of Askja adapted from [89] and showing the location of samples ASK 1-9. **(d)**  
253 Askja caldera from SE rim and ASK 5-9 sampling sites; **(e)** A1875, Layer 'D' [89] and capping  
254 lava flow; **(f)** TL sampling of Askja 1875 - ASK 5 (Layer 'C' [89] and ASK 6 (Layer 'D' [89]); **(g)**  
255 ASK 10 at Fiskidalur, 55 km NNE of Askja; **(h)** ASK 11 at Arnórsstaðamuli, 74 km NNE of Askja.  
256

257 **Óþoli Tephra:** The Óþoli tephra (ÓT) is a rhyolitic tephra deposit within a glacio-lacustrine  
258 sedimentary sequence near the plateau surface of Skagafjall [75, 97] (Fig. 5a–c). The ÓT  
259 sedimentary unit consists of 8-10 cm of airfall tephra overlain by up to c. 10 m of reworked  
260 volcanic ash (Fig. 5d). The airfall ash sub-unit is composed of more than 99% rhyolitic glass,  
261 with very minor basaltic–andesite/andesitic altered glass and sparse traces of feldspar, iron  
262 ore and pyroxene of uncertain origin [75, 97]. The 8–10 cm thick airfall ash is unusual for a  
263 tephra deposit on the NW (Vestfirðir) Peninsula, where visible tephra layers in Holocene peat  
264 deposits are uncommon, and usually less than a centimetre thick (Fig. 5d). Based on its  
265 stratigraphic position within an ice-dammed lake sequence in NW Iceland, the ÓT was  
266 originally thought to have been deposited c. 17–23 ka [97], but has since been dated to 2.26  
267 ± 0.11 Ma using the isothermal fission-track method [75]. Prior to fission-track dating analysis,  
268 preliminary luminescence experiments on the airfall rhyolitic glass fraction revealed the ÓT  
269 had a minimum age of at least c. 400 ka (Fig. 6f) [75]. The ÓT is most likely the product of a  
270 large Plinian-style eruption somewhere in the Húsafell region, a now inactive part of the SW  
271 Iceland axial rift (RVZ in Fig. 1) from near-central Iceland [75]. Prevailing north/north-north-  
272 westerly winds at the time of the eruption transported ash c. 200 km, depositing it on the  
273 heavily glaciated landscape of the Vestfirðir Peninsula during the Late Pliocene [75]. The  
274 A1875 tephra is the closest geochemical match to the Óþoli tephra (Figs. 1, S1) [75].



275

276 **Figure 5. Regional setting, stratigraphic logs and sampling of the Ópöli tephra. (a–c)** Location

277 of Skagafjall and main geological features of the Western Troughs of the Vestfirðir Peninsula



278 (based on [75, 97]). **(d)** Detailed stratigraphic log of and summary of palaeomagnetic results  
279 from Skagafjall section B units 10–12 and sampling strategy/sample numbers for the air fall  
280 and reworked components of the Ópoli tephra. Sample numbers 500-510 and 551-557 are  
281 SUTL laboratory numbers (SUERC-luminescence dating laboratory) sampled from the airfall  
282 tephra deposits in section B. SUTL558 is from section C. SUTL500-509 were sampled at 1 cm  
283 intervals from the basal 10 cm of Ópoli tephra above the rhythmite bed/tephra contact; UT  
284 sample numbers are University of Toronto fission-track laboratory numbers [97].

285

## 286 **Methods**

287 Luminescence dating relies on the laboratory reconstruction of the radiation dose absorbed  
288 by sensitive materials in the natural environment since formation or since the last heat- or  
289 light- induced resetting or ‘zeroing’ event [98–100]. For volcanic glass, the event being dated  
290 is the formation event, *i.e.*, cooling from magma, which due to its extremely high  
291 temperature, may be assumed to be free from residual thermoluminescence signals. Here,  
292 this assumption was verified, for practical purposes, using 19<sup>th</sup> Century material from the  
293 A1875 eruption. A laboratory determination of the total radiation dose experienced since the  
294 formation or last bleaching event is referred to as the equivalent or palaeodose,  $D_e$ . This is  
295 obtained, following measurement of the “natural” luminescence signal in the laboratory by  
296 reconstructing a stepwise luminescence dose-response curve by laboratory irradiation, and  
297 remeasurement of stimulated luminescence from purified sub-samples (or aliquot discs). If  
298  $D_T$ , the rate of radiation dose received by decay of radioactive elements, and cosmic  
299 radiation, *in-situ* in the natural environment, can be reliably assessed [99, 100], an age  
300 estimate can be determined, simply, as the quotient of palaeodose ( $D_e$ ) and environmental  
301 dose rate ( $D_T$ ) or  $[D_e / D_T]$ .

302

### 303 ***Sample collection and purification***

304 We examined the luminescence characteristics of undisturbed airfall deposits to avoid  
305 possible complications associated with post-depositional reworking and light exposure.  
306 Samples were collected by hammering light tight 22–27 mm diameter, 20–50 cm long copper  
307 tubes into airfall tephra and pumice deposits that had been cut back 10–30 cm. All samples  
308 were transported and stored under light-tight conditions and 2–5 cm of material at the end  
309 of the tubes that could have been exposed to light was removed.

310

311 Contaminant mineral phases that also retain a luminescence signal, such as quartz, feldspar  
312 and zircon, have a higher density ( $>2.45 \text{ g cm}^{-3}$ ) than rhyolitic glass ( $2\text{--}2.2 \text{ g cm}^{-3}$ ). Therefore,  
313 double-purified sieved 90–150  $\mu\text{m}$  volcanic glass fractions were prepared by density  
314 separation techniques [48, 73, 102]. Samples were cleaned ultrasonically in 10% hydrochloric  
315 acid (HCl) and density separated 2.3–2.4 or  $<2.4 \text{ g cm}^{-3}$  using sodium polytungstate solution  
316 (Figs. S1, S3). Harsh chemical treatments and etching were avoided due to the fragile nature  
317 of platey and pumiceous glass shards; hence, no attempt was made to clean the glass surfaces  
318 with hydrogen peroxide ( $\text{H}_2\text{O}_2$ ) or etch the shards with hydrofluoric acid (HF) to remove their  
319 thin outer layer influenced by external alpha-dose rates. Contamination by non-glassy phases  
320 was assessed using TL sensitivity response, and visually confirmed by light microscopy and  
321 Scanning Energy Dispersive-Scanning SEM (EDS-SEM) geochemical mapping of discs used in  
322 TL analysis and by examination of preliminary N/50 Gy dose response curves (Fig. 6, S4; see  
323 Supplementary Information for details).

324

### 325 ***SAR-TL experiment***

326 Based on findings from our preliminary experiments (Fig. 6; Supplementary Notes 2, 3), and  
327 after testing multiple aliquot methods [101], it was noted that the relatively high radiation  
328 doses needed to match natural signals from the early Quaternary Ópoli tephra analysis had  
329 potential to induce radiation colouring in the samples. Moreover, sensitivities in response to  
330 repeated 50 Gy irradiation and readout cycles tended to decline, suggesting that such  
331 radiation colouring was not being fully annealed by the TL heating cycle to 400 degrees. In  
332 recognition of this, to quantify equivalent doses and constrain ages for the Þórsmörk  
333 Ignimbrite and the Ópoli tephra, we adapted the Single-Aliquot Regeneration OSL (SAR-OSL)  
334 technique [103, 104] for TL analysis (SAR-TL) . In the SAR method, the same disc is exposed to  
335 a series of laboratory radiation doses prior to preheating and readout, followed by a test dose  
336 (TD) measurement to assess laboratory induced sensitivity changes across the measurement  
337 cycle. The natural TL was measured from purified glass on each disc, and TL was then  
338 artificially regenerated beyond the naturally accumulated TL by applying a series of laboratory  
339 radiation doses to each disc.

340

341 Stainless steel discs were cleaned with acetone and Electrolube SCO200D silicone grease then  
342 loaded with 4–6 mg of purified volcanic glass concentrated in the central area of each disc.  
343 Read-outs were undertaken using a Scottish Universities Environmental Research Centre  
344 (SUERC) TL Research Reader consisting of an Electron Tubes 9883 QB Photo-multiplier Tube  
345 (PMT) fitted with Schott 7/59 and KG1 filters and continuously flushed with nitrogen to  
346 prevent oxidising reactions that might create spurious TL. Measurements were undertaken  
347 manually with real time analysis to monitor glow shapes, assess integrated photon count  
348 rates to define successive regeneration doses levels required, and check for signal quality.  
349 Discs were heated from room temperature to 400 °C at 5 °C s<sup>-1</sup>. Blanks and blank

350 contamination discs were cleaned with acetone and sprayed with Electrolube SCO200D  
351 silicone grease, were placed on the work surface and read out at the end of each session.  
352 Discs for the N/50 Gy and SAR-TL experiment were irradiated using a shielded ELSEC 9022  
353 irradiator fitted with a 1.85 GBq  $^{90}\text{Sr}$   $\beta$ -ray source with a source to sample distance of 15 mm  
354 and a silicate dose rate of  $3.353 \pm 0.015 \text{ Gy min}^{-1}$  for the N/50 Gy experiment and  $3.270 \pm$   
355  $0.015 \text{ Gy min}^{-1}$  for the later SAR-TL experiments. Reconstructing the large natural signal  
356 retained in the Ópoli tephra proved particularly time consuming due to its large stored natural  
357 dose. For this experiment a higher dose rate irradiator incorporating a 11.1 GBq  $^{90}\text{Sr}$   $\beta$ -ray  
358 source at a working distance of 7.5 mm was used, yielding a mean dose rate in the central  
359 areas of the sample of  $32.0 \pm 0.6 \text{ Gy min}^{-1}$ . Both irradiators had been calibrated to high  
360 precision relative to the UK air kerma standards at the National Physical Laboratory (NPL)  
361 when commissioned in 1997, before this study.

362

### 363 ***SAR-TL Palaeodose reconstruction ( $D_e$ )***

364 After the natural TL signal had been thermally removed and measured (read-out), the TL and  
365 test dose and read-out measurement cycle for each disc consisted of: (1) Individual disc  
366 irradiation (PIG: 50, 75, 100, 125, 150, 200, 300 Gy; ÓT: 500, 1000, 1500, 2000, 3000, 4000,  
367 5000, 6000 Gy); (2) A short, high temperature (within-chamber) pre-heat of 220 °C for two  
368 minutes and 0–400 °C TL read-out; (3) Test-dose (TD), pre-heat, as stage 2, and 0–400 °C TL  
369 read-out. Disc-specific changes in sensitivity were in stage 3 were corrected by applying a test-  
370 dose (TD) after each successive regeneration dose (PIG = 25 Gy; ÓT = 100 Gy). Palaeodose ( $D_e$ )  
371 values for the Þórsmörk Ignimbrite PIG7 and the Ópoli tephra SUTL551 samples were  
372 calculated from standard error weighted regression of 200–400 °C, 10 °C integrated data  
373 (Tables 1, 2, S2, S4). The final weighted mean palaeodose values used in age estimates were

374 calculated from the most thermally stable peak intensity regions of the glow curve,  
375 determined by a  $D_e$  plateau plot. In summary,  $D_e$  values were integrated over three  
376 temperature regions that correspond to the wide (280–360 °C), median (290–330 °C) and  
377 narrow (290–310 °C) TL intensity peak region of the glow curves (Figs. 7–8; Tables 1, 2).  
378 Uncorrected (UC) and test-dose (sensitivity) corrected (TDC) regeneration curves, were  
379 modelled using best mathematical fit (highest adjusted  $r^2$  values,  $p$ -value <0.05) linear  
380 regression ( $y=ax+b$ ) and non-linear least squares saturating exponential regression analysis  
381 ( $y=a[1-e^{-bx}]$ ) applied to 10 °C interval datasets for both samples (Tables S2, S4). The non-  
382 linear and non-saturating response of the Ópoli Tephra was also modelled using saturating  
383 exponential + linear regression analysis ( $y=a[1-e^{-bx}] + cx$ ) [following 66]. Regression results  
384 shown in Tables 1 and 2 represent methods with the highest  $r^2$  and lowest RMSE values (see  
385 also Table S2, S4). Other regression models (e.g., saturating exponential, 2<sup>nd</sup> and 4<sup>th</sup> order  
386 polynomial) were investigated (e.g., Table S4). Regression and statistical analysis was  
387 undertaken in SigmaPlot (Systat Software Inc., San Jose California USA,  
388 [www.systatsoftware.com](http://www.systatsoftware.com)), XLSTAT (version 2010.3.09, [www.xlstat.com](http://www.xlstat.com)).

389

390 Fading tests were conducted at the end of the measurement cycle using multiple aliquot  
391 grouped approaches as suggested by Sanderson 1988 [116]. For this, two groups of discs were  
392 defined for each sample. As these had same prior radiation and TL readout histories as each  
393 other, both groups were expected to be in the same state, in respect of sensitivity and  
394 sensitisation behaviour. One of the groups was irradiated to a 50 Gy dose, at the start of the  
395 test period, and the other irradiated at the end of it –  $5 \times 10^6$  seconds. Both were preheated  
396 together, and then readout, in their 9<sup>th</sup> readout cycle since the start of the experiment. These  
397 results were normalised to those obtained from a prompt readout in their 8<sup>th</sup> cycle. By double

398 normalising the data sets and comparing the results from the two groups, the fading quotient  
399 associated with the dark storage for the period between prompt and stored readings was  
400 obtained. This approach provides for replication across many discs, and importantly is not  
401 affected by sensitivity changes in the samples (based on sensitisation between successive  
402 irradiation and readout cycles), or in the equipment (since the readout sessions for both  
403 groups of samples are conducted together both for the prompt and stored measurements).  
404 The fading observed crosses log time cycles 4-5 and 6-7.

405

406 A similar approach was adopted by Ward [67], who studied TL dose response, from 200 Gy to  
407 160 kGy, and stability of highly reproducible mass produced and fully melted silicate glass  
408 slices (i.e., microscope cover slips). Fading tests using high dose (44 kGy) covered 11  
409 logarithmically spaced post-irradiation intervals from 45 minutes after irradiation up to 35  
410 days. After an initial rapid fading over the first few hours following irradiation, subsequent  
411 losses diminished in rate as seen on a logarithmic time scale and appeared to be dominated  
412 by thermal fading processes. On this basis, the procedure adopted in the study aimed to avoid  
413 the immediate post-irradiation period. It is recognised that fading rates over longer  
414 Quaternary timescales represent an extrapolation over any observable laboratory storage  
415 test. Therefore, the results of the study were also be assessed relative to independent age  
416 controls of the Ópoli tephra and PIG in this study.

417

#### 418 ***Dose rate reconstruction ( $D_T$ )***

419 The overall dose rate to the tephra shards includes internally generated alpha and beta  
420 contributions, and externally delivered alpha, beta, gamma components from the bulk  
421 sediment matrix, which are attenuated by water, plus an external cosmic dose rate

422 component (Tables 3, 4). Bulk sample geochemical data, obtained by X-ray fluorescence (XRF)  
423 and Inductively Coupled Plasma-Mass Spectrometry (ICP-MS) analysis, was used to assess  
424 'external' or 'bulk' matrix dose-rates. Bulk dose rate calculations were based on the infinite  
425 matrix assumption [100], which states that samples are essentially homogeneous on a  
426 macroscale. Shard-specific electron probe microanalysis (EPMA) potassium (K) data and ICP-  
427 MS analysis of the purified glass fraction U, Th and Rb data were used for (internal) glass-  
428 shard dose rate calculations, ( $D_1^{\text{shard}}(\text{in-situ-sat})$ ) in Table 4, following [98, 100]. See  
429 Supplementary Note 1 for experimental procedures. We also compared dose rates derived  
430 from bulk and glass shard geochemistry with data derived from spectrometry measurements  
431 (Tables 3, 4, S5).

432

433 For the most realistic assessment of dose rate, we partitioned the shard alpha dose into an  
434 internal contribution, which is not subject to water-content attenuation, and an external  
435 alpha contribution, delivered across the pore space of the bulk matrix, which is attenuated by  
436 pore-water. For the final weighted mean glass-bulk dose rate model,  $D_1^{\text{glass-bulk}}(\text{in-situ-sat})$  (Table  
437 4), we partitioned the dose rate into internal glass shard and external matrix components  
438 according to water content attenuation as follows. Samples for this study were collected  
439 during the warmest and driest parts of the year. Since the Icelandic climate is significantly  
440 colder and wetter outside our sampling months of June-August, we defined the mean water  
441 content as the mid-point of the collected and saturated water content and applied a 15%  
442 error to cover possible fluctuations in water content during burial [following 105].

443

444 Dry dose rates were attenuated by appropriate factors before calculation of final 'wet' dose  
445 rates using equations in [100], as follows:  $\alpha\text{-wet} = \alpha\text{-dry} / (1 + 1.5\text{WF})$ ;  $\beta\text{-wet} = \beta\text{-dry} / (1 +$

446  $1.25WF$ );  $\gamma$ -wet =  $\gamma$ -dry /  $(1 + 1.14WF)$ , where  $W$  and  $F$  are as defined  $W = (\text{saturation wet}$   
447  $\text{weight} - \text{dry weight}) / (\text{dry weight})$ .  $F = \text{average fractional water content during burial history}$   
448  $\text{and was determined for two scenarios: as received water content (in-situ) and average}$   
449  $\text{palaeowater content, i.e., the mid-point between in-situ and saturated water content, with}$   
450  $\text{error limits that encompass the measured } F_{in-situ} \text{ and } W_{saturation} \text{ values. Errors in } F_{in-situ} \text{ are mean}$   
451  $\pm 1\sigma \text{ of three representative measurements, while } W_{saturation} \text{ errors are measurement errors}$   
452  $\text{from six duplicate measurements.}$

453

454 Internal (glass) and external (bulk) dose rates were based on geochemical and/or  
455 spectrometry data according to the following equations:  $D\alpha_T = k[\phi_g D\alpha_g + (1-\phi_M)WFD\alpha_M]$  and  
456  $D_{\beta T} = \phi_g D_{\beta} + (1-\phi_M)WFD_{\beta M}$ , where:  $\phi_g$ ,  $\phi_M$  are published absorbed dose factors and  $(1-\phi_M)$   
457 attenuation factors [107–109] that correspond to the median grain size for glass shards and  
458 matrix, respectively. Spectrometry-based dose rates were calculated from *in-situ* portable  
459 gamma-spectrometry, thick source beta counting (TSBC) and alpha spectrometry  
460 measurements (see Supplementary Note 4 for experimental details). Geochemical-based  
461 dose rates were calculated from bulk and shard-specific geochemical data in Tables 4 and S1  
462 using well-established conversion factors [109]. No thoron or radon loss was assumed in  
463 conversion calculations because samples are believed to be sufficiently compact. External  
464 attenuation factors for U, Th and K taken from [108] were based on a median grain-size of  
465  $100 \mu\text{m}$ . Equilibrium between U and Th decay was assumed as similarities between elemental  
466 and TSBC dose rates suggested that disequilibrium between decay products is minimal  
467 (Supplementary Note 4).

468

469 **Results**



470 ***Sample collection, purification & preliminary dose response screening***

471 We collected light-tight TL samples from 17 out of 23 locations visited in the Þórsmörk region  
472 (Figs. 2, 3). Samples covered a wide range of rhyolitic material, including pumice, airfall ash  
473 layers dominated by glass shards, inter-bedded rhyolitic ash layers associated with pyroclastic  
474 flow deposits, and reworked ash deposits overlying the pumiceous rich horizons (Fig. 3; Table  
475 S1). Sampled pumice clasts were unwelded and typically c. 10–50 cm in diameter (Fig. 3m).  
476 Ten light-tight samples were collected from airfall and reworked Óþoli tephra deposits (Fig.  
477 5). Light-tight samples of A1875 tephra were collected from three locations: 0.5 km SE of Víti  
478 within the caldera (ASK 5) (ash-rich layers C & D [90]), 55 km to the ENE of Víti at Fiskidalur  
479 (ASK 10), and 74 km NNE of Víti at Arnórsstaðamuli (ASK 11), where visible layers, up to 1 cm  
480 thick exist (Fig. 4). Ö1362 tephra samples were collected from three sites at 9 km (Kvísker),  
481 65 km (Hólmur), 86 km (Fóssdalur) to the East of the volcano along the principal eruption  
482 plume axis (Fig. 4). The major element geochemical composition of the rhyolitic glass-shards  
483 in the Ö1362 tephra is most similar to those of the Þórsmörk Ignimbrite (Fig. S1).

484

485 Visual inspection under the microscope revealed the rhyolitic ash and pumice Þórsmörk  
486 Ignimbrite samples were >95% glass, and the Óþoli tephra samples were >99% clear, platy  
487 glass shards of rhyolitic composition (Fig. 6). The bulk A1875 and Ö1362 samples were  
488 composed of >90–95% platy or pumiceous volcanic glass shards (Fig. 6). Þórsmörk Ignimbrite  
489 samples had the highest glass-shard alkali (Na+K) content of samples examined (Fig. S1). No  
490 purified fractions or SEM-EDS geochemical maps of discs used in SAR-TL experiments had  
491 exceptionally high K, Na, Ca, indicative of possible feldspar contamination (K, Na, Ca)AlSi<sub>3</sub>O<sub>8</sub>,  
492 (Fig. S5).

493

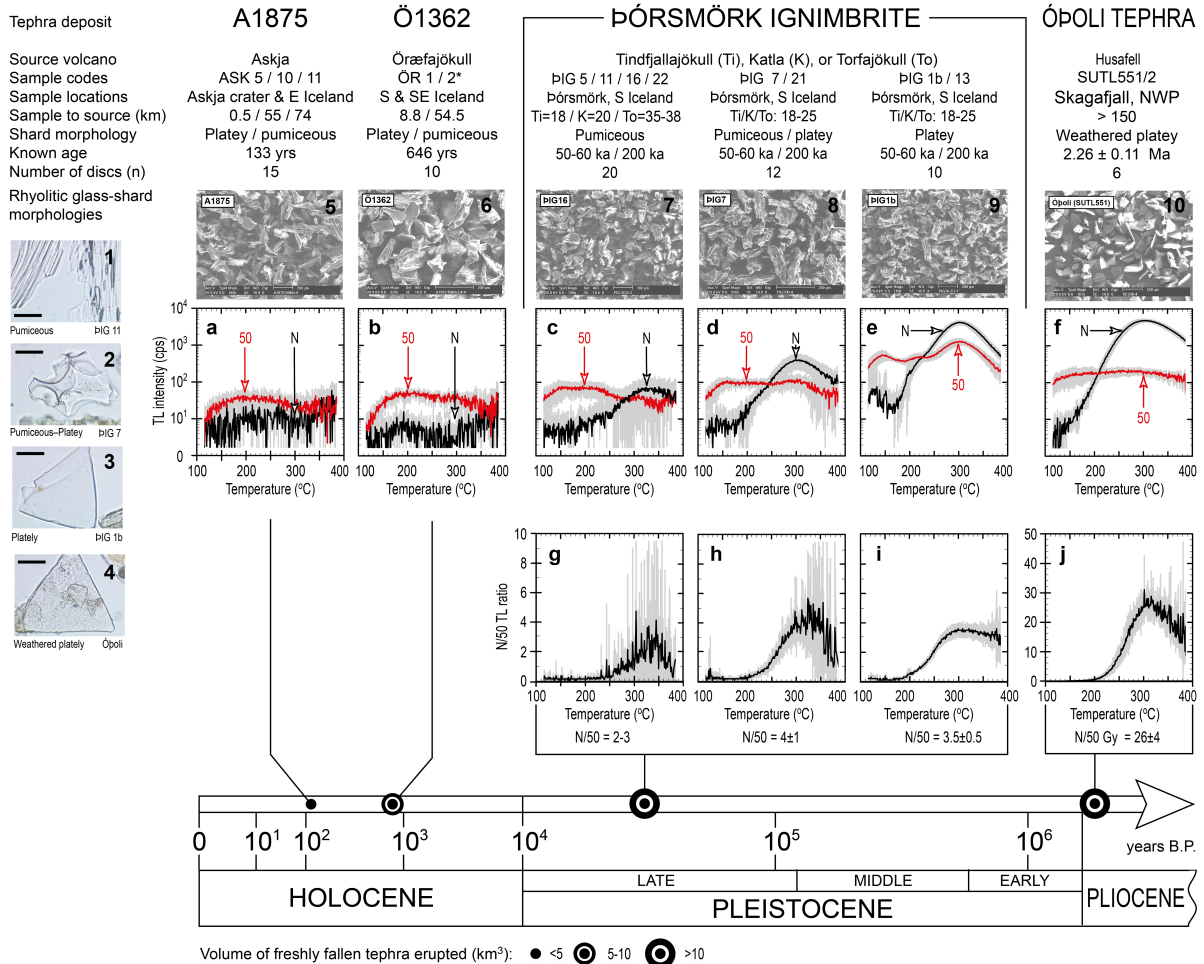
494 Using the purified 90-150 micron volcanic glass shard fraction of the four deposits, we  
495 thermally read out the natural signal and examined their response to a 50 Gy radiation dose.  
496 We also undertook TL bleaching, TL inducement and pre-heating tests (Figs. 6, S5;  
497 Supplementary Notes 2, 3). Results showed an age-related signal was retained by volcanic  
498 glass (Fig. 6), and that a fairly consistent volcanic glass-phase response to 50 Gy laboratory  
499 radiation dose existed across all samples. This was characterised by a broad peak intensity  
500 region of up to  $10^3$ – $10^4$  counts per second (cps) between 200–400 °C (Fig. 6a-d, f). The natural  
501 TL signal retained by the A1875 and Ö1362 samples was too small for further quantitative  
502 analysis using the existing set up (Fig. 6). Bleaching and inducement tests showed the TL signal  
503 could not be fully removed by optical exposure and that a TL signal of similar magnitude to  
504 the natural Ópoli tephra signal could not induced by optical exposure. Manual pre-heats of  
505 220 °C for two minutes, 155 °C for five hours or 135 °C for 16 hours all successfully removed  
506 the laboratory-induced low temperature (c. 110 °C) TL peak observed in the natural and 50  
507 Gy dose response experiment (Figs. 6, S5; see Supplementary Note 2 for experimental  
508 details).

509

#### 510 ***SAR-TL experiments & palaeodose reconstruction***

511 The Þórsmörk Ignimbrite ÞIG 7 purified glass sample was significantly more sensitive (defined  
512 as TL intensity per unit applied dose) than the Ópoli Tephra sample and had a straightforward  
513 linear dose response in the 200–400 °C temperature region (Figs. 7a, 8a). Notably, SAR-TL  
514 regression curves used for final analysis of the ÞIG7 and the Ópoli Tephra samples had mean  
515  $r^2$  values consistently  $>0.98$  with  $p < 0.0001$  in the 240–360 °C peak intensity region (Tables 1,  
516 2).

517



518

519 **Figure 6. Preliminary natural versus 50 Gy (N/50 Gy) dose response tests for purified**  
 520 **volcanic glass samples. (a)–(f)** black lines represent the mean natural TL intensity (N) in  
 521 counts per second (cps), at 1 °C intervals. Dark (red) lines represent the mean TL intensity  
 522 produced by applying a 50 Gy laboratory dose. Light grey lines are ± 1σ errors from n discs  
 523 shown at 1 °C intervals. Pre-heats were deliberately not applied prior to the N or 50 Gy TL  
 524 read outs to allow examination of the natural and dose response glow curve shape. This  
 525 creates a low temperature peak visible in some 50 Gy response profiles (e.g., ÞIG 1b and ÞIG  
 526 13). As no pre-heats or regression analysis were undertaken, the information contained in  
 527 this figure is not linked to age estimates obtained from the SAR-TL experiment. **(g)–(j)** Natural  
 528 and 50 Gy ratio plateau plots, showing the mean ratio and single standard deviation of the  
 529 N/50 Gy TL response; \* = ÖR 3 was visibly contaminated by minerals unrelated to the eruption

530 event and is not included for clarity. Microphotographs 1–4, taken at x400 magnification,  
531 illustrate the difference between pumice and platey glass shard morphologies; black scale bar  
532 is 25  $\mu\text{m}$ ; purified samples were mounted in Canada Balsam. Scanning Electron Microscope  
533 (SEM) microphotographs 5–10 show selected Ö1362, A1875, PIG7 and ÓT purified glass  
534 shards on discs used in the preliminary N/50 Gy experiment. Discs were carbon coated for  
535 SEM-EDS geochemical mapping causing low image resolution.

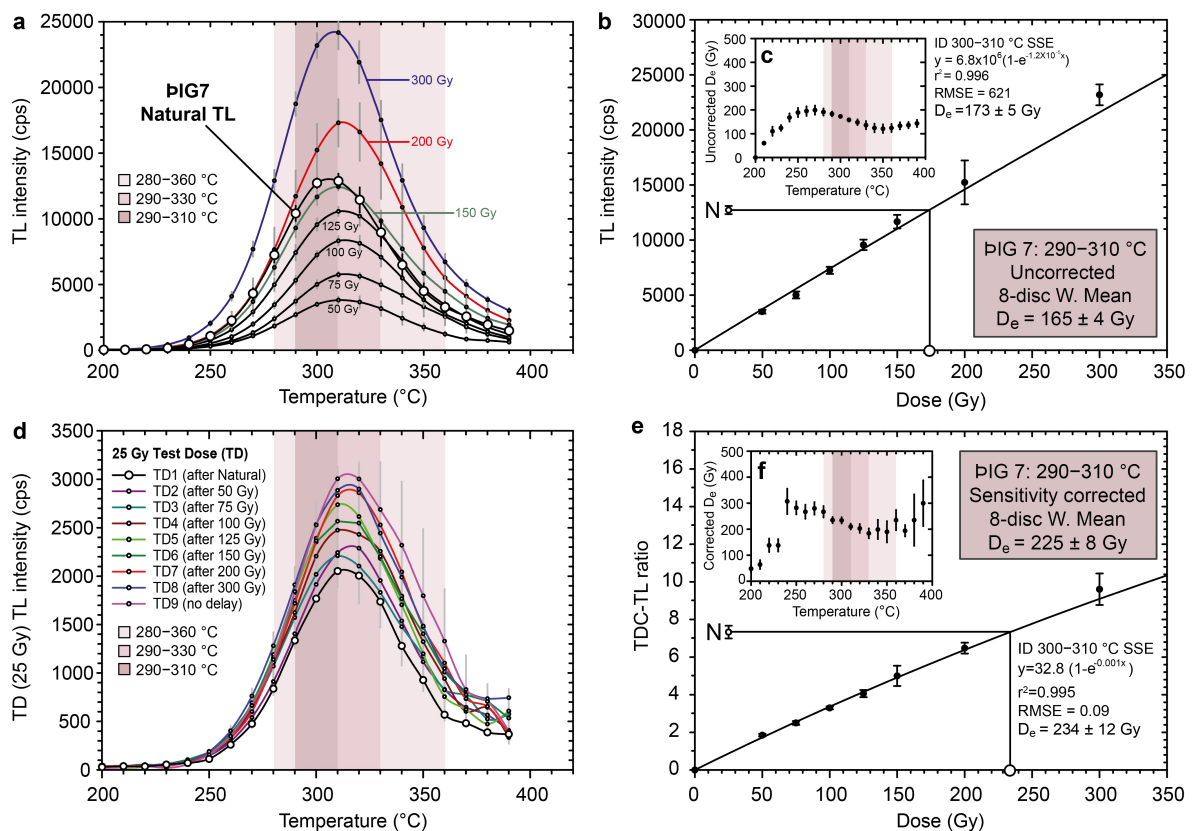
536

537 For PIG7, the uncorrected natural TL lies within an approximately linear growth phase of the  
538 regeneration curve, enabling reliable  $D_e$  values to be obtained by interpolation (Fig. 7b).  
539 Neither the type of regression curve fitted or the temperature integral chosen (280–360 °C ,  
540 290–330 °C or 290–310 °C peak intensity regions of the glow curve) made a significant impact  
541 on the reconstructed  $D_e$  value (Figure 7, Table 1). The PIG7 290–310 °C peak intensity region  
542 had the most stable  $D_e$  plateau region with the lowest measurement errors (Fig. 7c) and was  
543 chosen for  $D_e$  analysis. Uncorrected weighted linear (LIN) regression applied to 290–310 °C  
544 data produced a  $D_e$  value of  $169 \pm 4$  Gy, while weighted saturating exponential (SE) regression  
545 produced a  $D_e$  of  $165 \pm 4$  Gy (Fig. 7b; Table 1).

546

547 There was an approximately linear increase in TL intensity for PIG7 25 Gy test-doses TD1–TD9  
548 (Fig. 6a–b). The PIG7 test-dose sensitivity-corrected 290–330 °C peak intensity weighted  
549 mean  $D_e$  values were  $221 \pm 6$  Gy (LIN) and  $217 \pm 5$  Gy (SE) (Fig. 7e). Peak region (290–310 °C)  
550  $D_e$  values were similar ( $227 \pm 8$  Gy (LIN);  $225 \pm 8$  Gy (SE)). Athermal fading did not appear to  
551 be a significant for PIG7, with 96% of the signal retained in the 290–330 °C and 99% in the  
552 290–310 °C stable peak temperature regions after 60-day storage (Tables 1, S3). Test-dose  
553 (sensitivity) and 60-day storage loss-corrected SAR-TL  $D_e$  values across the 280–360 °C region

554 range from  $226 \pm 7$  Gy to  $234 \pm 11$  Gy (Table 1). The most accurate assessment of the PIG7  
 555 palaeodose is considered to be the weighted mean sensitivity and 60-day storage-corrected  
 556 SAR-TL  $D_e$  value of  $230 \pm 11$  Gy, obtained by weighted linear regression from the 290–310 °C  
 557 peak intensity temperature region (Table 1).



558  
 559 **Figure 7. SAR-TL palaeodose ( $D_e$ ) data for PIG 7 of the Þórs mörk Ignimbrite: (a)** Natural and  
 560 applied dose mean TL intensity glow curves. Weighted mean TL intensity standard  
 561 measurement errors were  $10.48 \pm 1.32\%$  in the 280–360 °C peak intensity region,  $5.93 \pm$   
 562  $0.66\%$  for 290–330 °C and  $5.95 \pm 0.95\%$  for 290–310 °C; **(b)** Example of a saturating  
 563 exponential (SE) weighted regression curve fitting of the form  $y=a[1-e^{(-bx)}$  in the peak TL  
 564 intensity 300-310 °C region. Similar SSE weighted regression was undertaken on 10-degree  
 565 interval data between 200–400 °C to generate the  $D_e$  plateau plot shown in (c) (Tables 1, S2);  
 566 **(c)** 200-400 °C  $D_e$  and temperature plateau plot; **(d)** 25 Gy test-dose (TD) mean TL intensity

567 glow curves; **(e)** Saturating exponential (SE) weighted regression of 300–310°C temperature  
 568 test-dose (sensitivity)-corrected data (see also Fig. S6); **(f)** 200–400 °C  $D_e$  temperature test-  
 569 dose (sensitivity) corrected  $D_e$  plateau plot. The weighted mean 290–310 °C sensitivity  
 570 corrected  $D_e = 225 \pm 8$  Gy. Results are based on 10 °C integration of original 1 °C data (Tables  
 571 1, S2).

Þórs mörk Ignimbrite Palaeodose Statistics & Age estimates				Weighted mean age (no fading correction) $(D_{e, \text{glass-bulk}})_{\text{in-situ-sat}} = 5.82 \pm 1.48$ (ka)	60-day storage loss correction (Fraction of signal retained)	60-day storage loss corrected weighted mean palaeodose $D_e \pm SE$ (Gy)	60-day storage loss corrected weighted mean age $(D_{e, \text{glass-bulk}})_{\text{in-situ-sat}} = 5.82 \pm 1.48$ mGy a <sup>-1</sup> (ka)	60-day storage loss corrected weighted mean age $(D_{e, \text{glass-bulk}})_{\text{in-situ-sat}} = 6.25 \pm 1.51$ mGy a <sup>-1</sup> (ka)	
ÞIG7 SAR-TL		Weighted mean palaeodose $D_e \pm SE$ (Gy)	8-Disc Mean Regression Error Analysis (all $p < 0.0001$ )						
	Mean $r^2 \pm 1\sigma$		Mean RMSE $\pm 1\sigma$						
Uncorrected	Linear regression								
	(a) 280-360 °C	157 ± 3	0.973 ± 0.025	639 ± 253	27 ± 7	<b>0.94 ± 0.04</b>	167 ± 8	29 ± 7	27 ± 7
	(b) 290-330 °C	166 ± 4	0.991 ± 0.009	527 ± 244	29 ± 7	<b>0.96 ± 0.02</b>	173 ± 5	30 ± 8	28 ± 7
	(c) 290-310 °C	169 ± 4	0.997 ± 0.003	352 ± 112	29 ± 7	<b>0.99 ± 0.03</b>	171 ± 7	29 ± 8	27 ± 7
	Saturating exponential regression								
	(d) 280-360 °C	151 ± 3	0.987 ± 0.009	511 ± 93	26 ± 7	<b>0.94 ± 0.04</b>	160 ± 8	28 ± 7	26 ± 6
Test dose- (Sensitivity)- corrected	(e) 290-330 °C	158 ± 3	0.995 ± 0.003	543 ± 62	27 ± 7	<b>0.96 ± 0.02</b>	165 ± 5	28 ± 7	26 ± 6
	(f) 290-310 °C	165 ± 4	0.997 ± 0.003	528 ± 65	28 ± 7	<b>0.99 ± 0.03</b>	167 ± 7	29 ± 7	27 ± 7
	Linear regression								
	(a) 280-360 °C	220 ± 5	0.984 ± 0.018	### ± 0.05	38 ± 10	<b>0.94 ± 0.04</b>	234 ± 11	40 ± 10	37 ± 9
	(b) 290-330 °C	221 ± 6	0.996 ± 0.004	### ± 0.03	38 ± 10	<b>0.96 ± 0.02</b>	231 ± 8	40 ± 10	37 ± 9
	(c) 290-310 °C	227 ± 8	0.999 ± 0.001	### ± 0.03	39 ± 10	<b>0.99 ± 0.03</b>	230 ± 11	39 ± 10	37 ± 9
Saturating exponential regression									
(d) 280-360 °C	215 ± 5	0.993 ± 0.009	### ± 0.06	37 ± 9	<b>0.94 ± 0.04</b>	229 ± 11	39 ± 10	37 ± 9	
(e) 290-330 °C	217 ± 5	0.999 ± 0.001	### ± 0.04	37 ± 10	<b>0.96 ± 0.02</b>	226 ± 7	39 ± 10	36 ± 9	
(f) 290-310 °C	225 ± 8	0.999 ± 0.001	### ± 0.05	39 ± 10	<b>0.99 ± 0.03</b>	228 ± 10	39 ± 10	36 ± 9	

572

573 **Table 1. Summary palaeodose statistics and age estimates for the ÞIG7 sample.** The

574 weighted mean test-dose (sensitivity) and 60-day storage-loss corrected palaeodose and age

575 estimates shown in dark grey and in bold are considered to be reliable. Best fit regression

576 analysis was determined from highest adjusted  $r^2$  values. Ten-degree integrated ranges for

577 the 280–360 °C, 290–330 °C and 290–310 °C TL peak intensity regions are shown. The 290–

578 310 °C and 290–330 °C ranges (dark grey shading) have the lowest TL intensity measurement

579 errors, the highest 8-disc mean  $r^2$ , lowest RMSE values and lowest  $p$ -values. This produced

580 sensitivity and 60-day storage loss corrected palaeodoses of c. 230 ± 10 Gy and ages of 40 ±

581 10 ka. Data have been rounded to the nearest 10 Gy and 5 ka to reflect calculation errors,

582

583 In the 50 Gy dose response screening experiment, the natural TL signal from the Óþoli tephra

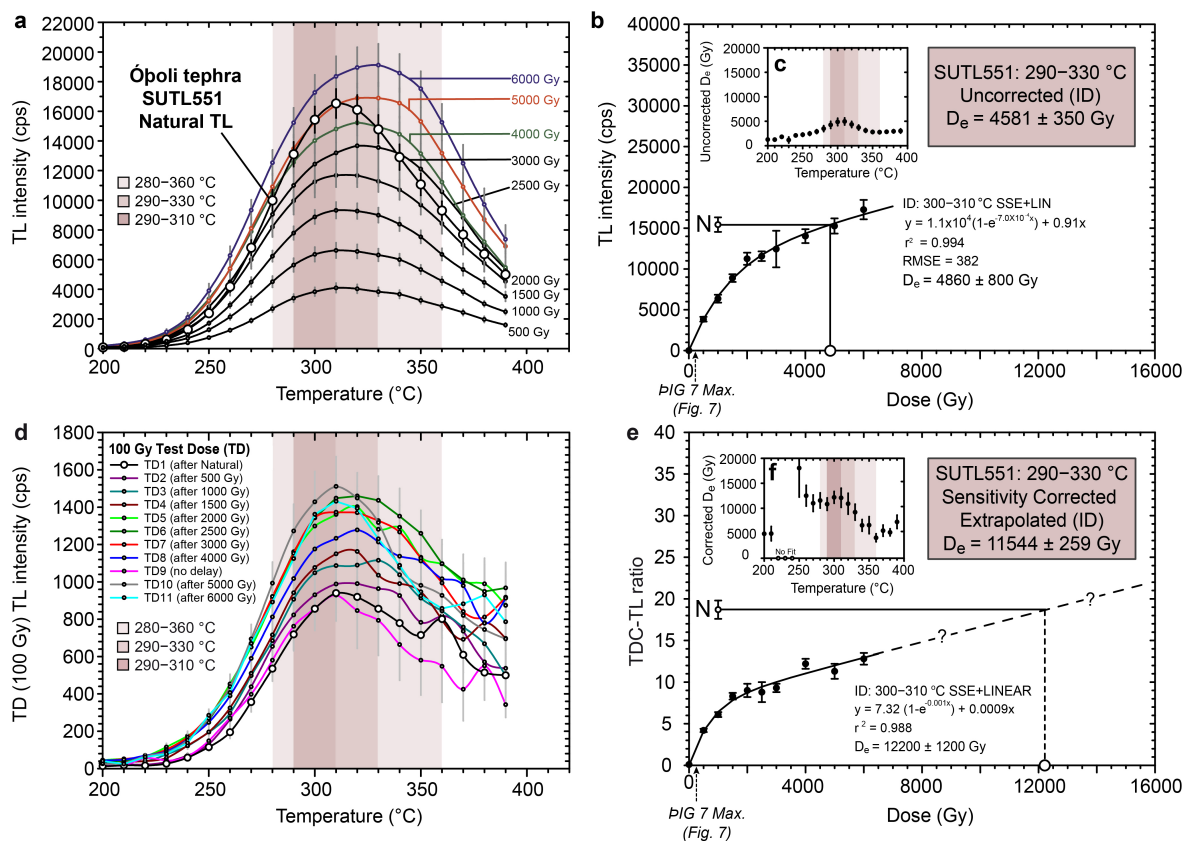
584 formed ‘broad’ unimodal peak of  $10^3$ – $10^4$  cps °C<sup>-1</sup> between 280–360 °C (Fig. 6), indicating a

585 TL signal that is predominantly stored in the more stable, longer-term energy traps evicted at  
586 high temperature. In the SAR-TL experiment, the uncorrected natural TL peak intensity region  
587 of the glow curves from the Ópoli tephra (ÓT) covered a broader temperature range, 290–  
588 330 °C, than PIG 7 (Fig. 8a). The broader shape of the regeneration dose response curve alone  
589 implied that the ÓT was significantly older than the PIG7 sample (Fig. 8b). Regression results  
590 show that the ÓT natural signal was located in an approximately linear growth phase *after* an  
591 initial non-linear growth phase, best modelled by a saturating exponential plus linear  
592 regression fit (Fig. 8b; Table S4). We chose this type of regression because it had a consistently  
593 higher  $r^2$  and lower RMSE values than single saturating exponential or polynomial (quadratic)  
594 regression models (290–330 °C region mean  $\pm 1\sigma$   $r^2 = 0.995 \pm 0.001$ ;  $p < 0.0001$ ; Figs. 8b, S6;  
595 Tables 2, S4). The 290–330 °C peak intensity region had the most stable  $D_e$  plateau, and  
596 produced a weighted mean  $D_e$  value of  $4581 \pm 350$  Gy (Fig. Table 2).

597

598 Assessing sensitivity change for the ÓT was more complex than for PIG7, with TL intensity  
599 reversals between some adjacent 100 Gy test-dose runs (Fig. S6c–d). These non-linear effects  
600 could be due to the (age-related) highly weathered and comparatively hydrated state of the  
601 ÓT glass shards, the high laboratory dose rate, the higher magnitude of applied doses (>1  
602 kGy), and/or cumulative radiation induced sensitivity changes (such as radiation ‘colouring’).  
603 If the ÓT test-dose corrected response curve continued to grow in the same approximately  
604 linear manner beyond 6 kGy, an applied dose in excess of 10 kGy would be required to  
605 produce an interpolated sensitivity-corrected palaeodose estimate (Fig. 8e; Table 2). It was  
606 not possible to apply such a high dose in the time available. Moreover, athermal fading  
607 appeared to be a significant factor for the ÓT sample examined, with 73% the signal retained

608 in the 290–330 °C and 79% retained in the 290–310 °C stable peak temperature regions after  
 609 60-day storage (Tables 2, S3).



610  
 611 **Figure 8. SAR-TL  $D_e$  data for the Ópoli tephra airfall ash sample SUTL551: (a) Natural and**  
 612 **applied dose mean TL intensity glow curves. Weighted mean uncorrected TL intensity**  
 613 **measurement errors were  $6.40 \pm 0.11$  % for the 280–360 °C peak intensity region,  $6.37 \pm$**   
 614  **$0.06$ % for 290–330 °C and  $6.40 \pm 0.13$ % for 290–310 °C; (b) Example of a saturating**  
 615 **exponential (SE) plus linear (LIN) weighted regression curve fitting  $y = a[1 - e^{-bx}] + cx$  in the peak**  
 616 **TL intensity 300–310 °C region. Similar SSE+LIN weighted regression was undertaken on 10**  
 617 **degree interval data between 200–400 °C to generate the  $D_e$  plateau plot shown in (c) (Tables**  
 618 **2, S4); (c) 200–400 °C  $D_e$  vs temperature plateau plot; (d) 100 Gy test-dose (TD) mean TL**  
 619 **intensity glow curves; (e) SE+LIN weighted regression of 300–310 °C temperature peak region,**  
 620 **highlighting how the reconstructed natural test-dose (sensitivity) corrected is greater than**



621 the highest applied dose of 6000 Gy (see also Fig. S6); **(f)** 200–400 °C ( $D_e$ ) test-dose (sensitivity)  
 622 corrected palaeodose ( $D_e$ ) plateau plot. Results shown are based on 10 °C integrals with  
 623 standard measurement error from measured 1 °C data (see also Tables 1, S3, S4).

Ópoli Tephra Palaeodose Statistics & Age estimates					Weighted mean age (no fading correction) $(D_T^{\text{glass-bulk}})_{\text{in-situ-sat}} 2.83 \pm$ (ka)	60-day storage loss correction (Fraction of signal retained)	60-day storage loss corrected weighted mean palaeodose $D_e \pm SE$ (Gy)	60-day storage loss corrected weighted mean age estimate $(D_T^{\text{glass-bulk}})_{\text{in-situ-sat}} 3.97 \pm 0.47$ (ka)	60-day storage loss corrected weighted mean age estimate $(D_T^{\text{glass-bulk}})_{\text{in-situ-sat}} 2.83 \pm$ (ka)
Ópoli Tephra (SUTL 551) SAR-TL		Weighted mean palaeodose $D_e \pm SE$ (Gy)	8-Disc Mean (8DM) Regression Error Analysis (all $p < 0.0001$ ) Mean $r^2 \pm 1\sigma$ Mean RMSE $\pm 1\sigma$						
Uncorrected	(a) 280-360 °C	3335 ± 155	0.995 ± 0.0015	331 ± 26	1178 ± 100	0.74 ± 0.03	4505 ± 278	1135 ± 90	1592 ± 149
	(b) 290-330 °C	4581 ± 350	0.995 ± 0.0012	342 ± 29	1619 ± 168	0.73 ± 0.02	6294 ± 511	1585 ± 151	2224 ± 239
	(c) 290-310 °C	4549 ± 524	0.995 ± 0.0002	355 ± 38	1607 ± 217	0.79 ± 0.01	5764 ± 668	1452 ± 184	2037 ± 277
Test-dose (Sensitivity) corrected	(a) 280-360 °C	8173 ± 153	0.986 ± 0.003	0.68 ± 0.13	2888 ± 211	0.74 ± 0.03	##### ± 493	-	-
	(b) 290-330 °C	##### ± 259	0.988 ± 0.003	0.58 ± 0.09	4079 ± 302	0.73 ± 0.02	##### ± 562	-	-
	(c) 290-310 °C	##### ± 302	0.986 ± 0.003	0.63 ± 0.09	4077 ± 307	0.79 ± 0.01	##### ± 426	-	-

624

625 **Table 2. Summary palaeodose statistics and age estimates for the Ópoli tephra, sample.**

626 Ten-degree integrated intensity ranges for the three peak temperature plateau regions 280–  
 627 360 °C, 290–330 °C and 290–310 °C are shown. The weighted mean sensitivity and 60-day  
 628 storage loss-corrected palaeodose and age estimates highlighted in light grey overlap the  
 629 fission-track age of  $2.26 \pm 0.11$  Ma [75].

630

631 ***Dose rates and age estimates***

632 Environmental dose rates for PIG7, PIG1b and Ópoli tephra samples shown in Tables 3, 4 and  
 633 S5 were produced using well-established equations and dose rate conversion factors. For  
 634 PIG7, the spectrometry-based dose rate of  $5.82 \pm 1.48$  mGy  $a^{-1}$  and geochemistry-based dose  
 635 rate of  $6.25 \pm 1.51$  mGy  $a^{-1}$  in combination with the sensitivity and 60-day storage loss-  
 636 corrected palaeodose values of c.  $230 \pm 10$  Gy produced age estimate of  $40 \pm 10$  ka. High  
 637 errors of c. 25% are mainly due to large uncertainties associated with estimating palaeowater  
 638 content fluctuations. Due to erratic changes in sensitivity and unresolved, but significant,  
 639 athermal signal losses, we cannot currently reconstruct a reliable SAR-TL age estimate for the  
 640 Ópoli tephra sample. Interestingly, though, the minimum uncorrected age shown in Table 2

641 is  $1178 \pm 100$  ka or  $1.18 \pm 0.1$  Ma, and the 60-day storage loss-corrected SAR-TL  $D_e$  value of  
 642  $6294 \pm 511$  Gy and a geochemical dose-rate of  $2.83 \pm 0.41$  mGy  $a^{-1}$  produces an age estimate  
 643 of  $2,224 \pm 239$  ka ( $2.22 \pm 0.24$  Ma) (Table 2), which is similar to the Ópöli tephra glass-shard  
 644 fission-track age of  $2.26 \pm 0.11$  Ma [75].

Geochemistry		Latitude	Longitude	Sampling	$D_{\text{cosmic}}^1$ dose rate (mGy $a^{-1}$ )	Elemental concentrations				
Tephra	Matrix	(°N)	(°W)	Depth (m)		n	K or $K_2O^*$ (wt %)	U (ppm)	Th (ppm)	Rb (ppm)
<b>Pörsmörk Ignimbrite</b>										
PIG 7	Bulk	63°40.37	19°34.37	1 ± 0.5	0.16 ± 0.06	-	3.03 ± 0.15	3.80 ± 0.19	13 ± 0.7	107 ± 5
	Glass					20	4.07 ± 0.19*	4.37 ± 0.22	14.3 ± 0.7	-
PIG 1b	Bulk	63°40.35	19°36.22	20 ± 5	0.04 ± 0.01	-	3.28 ± 0.16	3.13 ± 0.16	10 ± 0.5	73 ± 4
	Glass					24	4.11 ± 0.61*	3.39 ± 0.17	11.6 ± 0.6	-
<b>Ópöli Tephra</b>										
SUTL551/2	Bulk	65°59.78	23°45.40	5 ± 1	0.11 ± 0.04	-	2.16 ± 0.11	2.26 ± 0.03	8.5 ± 0.4	55 ± 3
	Glass					137	2.75 ± 0.14*	2.60 ± 0.10	10.8 ± 0.5	-

645

646 **Table 3. Location and geochemical data used to calculate dose rates for the Pörsmörk**  
 647 **Ignimbrite and Ópöli tephra samples.** <sup>1</sup>The cosmic dose rate calculation assumes no change  
 648 in sediment depth throughout burial and was calculated from  $0.21e^{[-0.07(dr)+0.0005(dr)^2]}$  mGy  
 649  $a^{-1}$  [following 130] where d is current depth of burial and r is the density of the attenuating  
 650 medium where  $r = 0.998$  g  $cm^{-3}$  for water and  $2.6$  g  $cm^{-3}$  were used for sediment; n = number  
 651 of shards analysed (Supplementary Note 1 and Table S1 for details).

Dose rate data		Glass shard dose rates					Bulk matrix dose rates					Weighted mean
Tephra	Measurement	$D_{\alpha_T}$	$D_{\beta_T}$	$D_{\gamma_T}$	$D_{\text{cos}}$	$(D_T^{\text{glass}})_{(in-situ\ to\ sat)}$	$D_{\alpha_T}$	$D_{\beta_T}$	$D_{\gamma_T}$	$D_{\text{cos}}$	$(D_T^{\text{bulk}})_{(in-situ\ to\ sat)}$	$(D_T^{\text{glass-bulk}})_{(in-situ\ to\ sat)}$
Lab ID	technique	(mGy $a^{-1}$ )				(mGy $a^{-1}$ )	(mGy $a^{-1}$ )				(mGy $a^{-1}$ )	
<b>Pörsmörk Ignimbrite</b>												
PIG 7	$\alpha$ -dose excluded	-	-	-	-	-	-	2.81	1.07	0.16	2.85 ± 0.60	2.85 ± 0.60
	Spectrometry*	1.84	2.12	1.09	0.16	5.22 ± 2.11	3.04	2.12	1.07	0.16	6.39 ± 2.07	5.82 ± 1.48
	Geochemical	1.84	2.09	1.09	0.16	5.18 ± 2.38	3.04	3.32	1.09	0.16	6.97 ± 1.96	6.25 ± 1.51
PIG 1b	$\alpha$ -dose excluded	-	-	-	-	-	-	2.55	1.09	0.05	2.96 ± 0.57	2.96 ± 0.57
	Spectrometry*	1.72	1.91	1.11	0.04	4.78 ± 2.12	2.43	1.91	1.09	0.05	5.48 ± 2.03	5.14 ± 1.47
	Geochemical	1.71	2.30	1.11	0.05	5.17 ± 2.64	2.43	3.12	1.11	0.05	6.71 ± 2.14	6.10 ± 1.66
<b>Ópöli Tephra</b>												
	$\alpha$ -dose excluded	-	-	-	-	-	-	1.59	0.56	0.11	1.83 ± 0.17	1.83 ± 0.17
	Spectrometry*	1.30	1.11	0.30	-	2.70 ± 0.62	1.51	1.11	0.30	-	2.92 ± 0.54	2.83 ± 0.41
	Geochemical	1.30	1.65	0.85	0.11	3.90 ± 0.66	1.51	1.58	0.85	0.11	4.04 ± 0.67	3.97 ± 0.47

652

653 **Table 4. Summary dose rate data for the Pörsmörk Ignimbrite and Ópöli tephra samples.**  
 654 Summary dose rate values were calculated with  $\alpha$ -dose rate excluded, using spectrometry  
 655 data ( $\alpha$ -dose included) and using geochemical data ( $\alpha$ -dose included) for three scenarios:

656 glass shard, bulk matrix, and weighted mean (glass shard–bulk) matrix. Values in bold are  
657 considered most likely. For geochemical calculations, the glass shard matrix dose rate was  
658 calculated using well-established equations and conversion factors [107–109, 130–133]. Since  
659 the biggest source of uncertainty is variations in palaeowater content, using more recent  
660 conversion factors does not significantly alter these calculated dose rates or errors. Total  
661 alpha, beta and gamma dose rates ( $D\alpha_T$ ,  $D\beta_T$ ,  $D\gamma_T$ ) incorporate attenuation factors based on  
662 *in situ*–saturation water content values [105, 132], which we consider to be most  
663 representative of the average water content through burial history at both the ÞIG 7 and Óþoli  
664 tephra sites (see Methods, Table S5).  $D_{cos}$  is the cosmic dose rate shown in Table 3. Errors for  
665 dose rate components are not shown for clarity but are typically  $\pm 10\%$ .

666

## 667 **Discussion**

668 We discuss the accuracy of the new ÞIG7 TL age estimate, examine implications of the age  
669 obtained, and make suggestions for future TL analysis of glass-rich tephra deposits based on  
670 the results from the ÞIG7 and Óþoli tephra experiments.

671

## 672 **Experimental Implications**

673 Our experiments on the Þórsmörk Ignimbrite (ÞIG7) produced age estimates that were similar  
674 orders of magnitude to published ages, highlighting that a glass-formation age-related TL  
675 signal is retained by the rhyolitic volcanic glass component of Icelandic tephra. In palaeodose  
676 reconstruction, even the smallest laboratory doses are applied at rates which are several  
677 orders of magnitude greater than those experienced in the natural environment. This creates  
678 two problems. First, high laboratory doses tend to fill or saturate shallow, thermally unstable  
679 traps, a process which does not occur during slower natural irradiation processes and may

680 result in differences in deep trap sensitivity [99, 110, 111]. Second, although laboratory dose  
681 rates less than c. 10 Gy min<sup>-1</sup> are not thought to be problematic [100], studies have shown  
682 that laboratory irradiation at 10<sup>8</sup>–10<sup>11</sup> (c. 0.1–100 Gy min<sup>-1</sup>) times greater than that  
683 experienced in the natural environment can lead to defect creation, migration and,  
684 ultimately, defect complex creation, which does not occur naturally [121]. Glass should be  
685 one of the materials least affected, because localised charge transport is not favourable for  
686 shallow-deep trap competition. The erratic sensitivity changes observed for the Ópoli tephra  
687 in the SAR-TL experiment suggest the comparatively higher laboratory dose rates (an order  
688 of magnitude greater than for the PIG7 sample) were detrimental in this respect. The obvious  
689 solution is to reduce the applied dose rate, but this would be extremely time consuming for  
690 multiple discs with several applied doses runs >1000 Gy.

691

692 Further investigation into the influence of sample age and applied dose on athermal signal  
693 loss is recommended. This effect was minimal for the PIG sample but appears to be a  
694 significant issue for the much older Ópoli tephra, which received applied doses in the c. 1-6  
695 kGy range. From our investigations, the athermal signal loss characteristics of ‘younger’  
696 volcanic glass deposits appears to be similar to those of commercial glasses, which do not  
697 exhibit significant athermal losses at ‘low’ applied doses i.e., <100 kGy [66]. Compositional  
698 differences, additional lattice defects and/or weathering could explain the lower dose  
699 threshold observed in our experiments.

700

701 Athermal fading of stored TL in phenocrysts of volcanic origin is thought to be responsible for  
702 significant D<sub>e</sub> underestimates in OSL dating of quartz phenocrysts present in some tephra  
703 deposits from Japan [112, 114, 115] and infra-red stimulated luminescence (IRSL) dating of

704 volcanic feldspar and other phenocrysts in the Old Crow Tephra, Alaska [113]. 'Young' volcanic  
705 glass shards appear less susceptible to long-term athermal signal loss at low irradiation doses  
706 [65, 66, 110-115], perhaps because fewer opportunities for long-range charge transport exist  
707 in volcanic glass compared to mineral-based luminescence systems. The relatively small TL  
708 signals per unit dose and low short-range order of glasses may also result from increased  
709 opportunities for competing non-radiative relaxation. At low doses, recombination is most  
710 likely to take place in hole centres populated from non-correlated ionising events, leading to  
711 the type of reproducible dose response curves observed in the PIG7 sample. At higher doses  
712 (*e.g.*, >1 kGy) [66], the increased proximity between donors and acceptors pair may eventually  
713 favour tunnelling recombination and limit stability, as seen by the greater athermal losses in  
714 the Ópoli tephra.

715

716 By calculating the ionisation density as a function of dose, and partitioning the dose (energy  
717 per unit mass) amongst the atoms in feldspar, Sanderson [116] showed that the mean spacing  
718 of randomly positioned charge-carriers in a lattice irradiated at low doses was greater than  
719 1000 lattice units. The random spatial model for fading in calcite [117], which has been  
720 subsequently applied to feldspars [116, 118], other minerals [119], and volcanic products  
721 [120] is perhaps less relevant for volcanic glass since it cannot support high rates of tunnelling  
722 at low dose without some form of charge-defect clustering, leading to deviations from the  
723 logarithmic ( $1/t$ ) decay behaviour predicted by the Visocekas [117] model. Ward [66] showed  
724 that fading from glass cover slips across a range of doses up to 160 kGy exhibits logarithmic  
725 ( $1/t$ ) decay behaviour only at the highest doses used. At very high doses, the proximity of  
726 neighbouring ion pairs becomes sufficiently close to enable anomalous signal losses from the  
727 glass matrix by quantum mechanical tunnelling [cf. 116], as observed by high dose

728 experiments from glass slices [66, 111]. In fact, all materials should exhibit (quantum  
729 mechanical) tunnelling as the number of mean concentration of electron-ion pairs reaches  
730 the percent level. If 1 kGy corresponds to 10 ppm initial ionisation, the mean concentration  
731 of electron-ion pairs reaches the percent level at doses in the 10's-100's kGy region. At low  
732 doses, thermal fading occurs from the continuum of traps where charge is located, and is  
733 presumably lost to non-luminescence processes, but this is not necessarily a significant  
734 barrier to successful dating providing the stability of the signal can be demonstrated by, for  
735 example, the existence of stable thermal plateau plots.

736

737 In early work examining a range of glass-rich tephras Berger [73,74], expressed concern that  
738 feldspar phenocrysts had potential to dominate fading behaviour for impure samples. He  
739 noted the apparent stability of the glass rich tephra from the Mazama, tephra and suggested  
740 that the glass phase experienced long-term athermal fading. Following the demonstration  
741 that tephra showed weak OSL and IRSL response [75], Auclair [113] studied the potential of  
742 IRSL dating from Crow Lake tephra from Alaska, in conjunction with stratigraphically  
743 associated loess. The tephra samples, which had not been subject to flotation, had IRSL signals  
744 which were an order of magnitude lower than the glass rich fractions, but, unlike samples used  
745 in this study, retained plagioclase as well as volcanic glass, pyroxene and iron oxides. Three  
746 approaches to fading analysis over a timescale ranging from 16 hours to 2000 hours were  
747 examined, with differing results. When aliquots were irradiated and staggered intervals and  
748 read together at the end of the storage period (to minimise the effects of sensitivity change  
749 in readout equipment), scattered results were obtained, with a mean value of 2% fading per  
750 decade of time. The use of short IRSL measurements, which scarcely depleted individual  
751 aliquots, allowed multiple measurement from individual samples, and produced more

752 coherent data. Fading rates of 4% and 6% per decade were obtained from loess and tephra  
753 samples, which are within uncertainties of each other. These values are very similar to values  
754 obtained from feldspars. Auclair [113] noted the possibility that they may relate to the  
755 phenocrysts in the sample, rather than the glass phase, and also noted the possible ambiguity  
756 between fading and sensitivity change in the experimental design.

757

758 While our experiments suggest that the purification of coarser material from both PIG7 and  
759 the Ópoli tephra was more successful, at this stage, it is not clear if storage signal losses  
760 observed from the Ópoli tephra were due to insufficient thermal stability in the temperature  
761 range examined, the onset of proximity effects or possibly related to the increased level of  
762 weathering experienced by this sample over time. Despite low luminescence sensitivities, the  
763 signal obtained from synthetic glasses continued to grow in a similar approximately linear  
764 fashion after near-saturation to the Ópoli tephra [66]. This implies that dating of volcanic glass  
765 up to at least two million years old could be possible, but several technical refinements are  
766 needed to obtain accurate and reliable ages. Further high-dose experiments on volcanic glass  
767 of Quaternary age and different geochemical composition are recommended to determine if  
768 signal loss is related to burial age, geochemical composition and/or the scale of laboratory  
769 doses or dose rates.

770

771 The other key factor in assessing the reliability of age estimates is the accuracy of calculated  
772 dose rates. The large age errors in this study relate to the large dose rate errors and are  
773 primarily due to long-term variations in palaeowater content during burial. However, our  
774 dose rate calculations also had to account for variations in the alpha dose contribution since  
775 it was not possible to etch the thin platy glass shards without destroying them. The alpha

776 dose contributed as much as 50% of the total dose rate in this study and creates uncertainties  
777 that are as significant as those associated with changes in palaeowater content (Table 4). The  
778 observed similarity between bulk and internal glass-shard compositions in both samples  
779 examined suggests that sharp micro-dosimetric discontinuities probably do not exist at shard  
780 boundaries. Nevertheless, whilst we constrained alpha dose-related uncertainties as far as  
781 currently feasible, alpha dose attenuation in irregularly shaped glass shards could be  
782 significantly different to published dosimetric equations, which are based on spherical grains  
783 [100, 108, 122, 123]. Numerical modelling, beyond the scope of this paper, is therefore  
784 recommended to fully evaluate the dosimetric properties of glass shard shapes that are not  
785 perfect spheres. An in-depth comparison with dose rates from tephra deposits where volcanic  
786 glass constitutes less than c. 95% of the bulk tephra matrix might also be useful.

787

788 In summary, we conclude that sensitivity and long-term storage tests are critical components  
789 that should be included in all future analyses. Further reducing uncertainties associated with  
790 our age estimates would also require extensive *in-situ* dose rate measurements, including for  
791 example, a better assessment of seasonal to multi-decadal fluctuations in water content at  
792 each site. Automation, single-grain glass shard analysis (where sensitivity allows) and pulsed-  
793 laser infra-red stimulated luminescence (IRSL) methods could be applied and compared to  
794 ages obtained from feldspar-phenocryst phases in glass-rich deposits. This could result in  
795 reliable TL ages from tephra across a broad age-spectrum, up to and beyond the radiocarbon  
796 dating upper limit of c. 50 ka.

797

798 ***Palaeoenvironmental Implications***

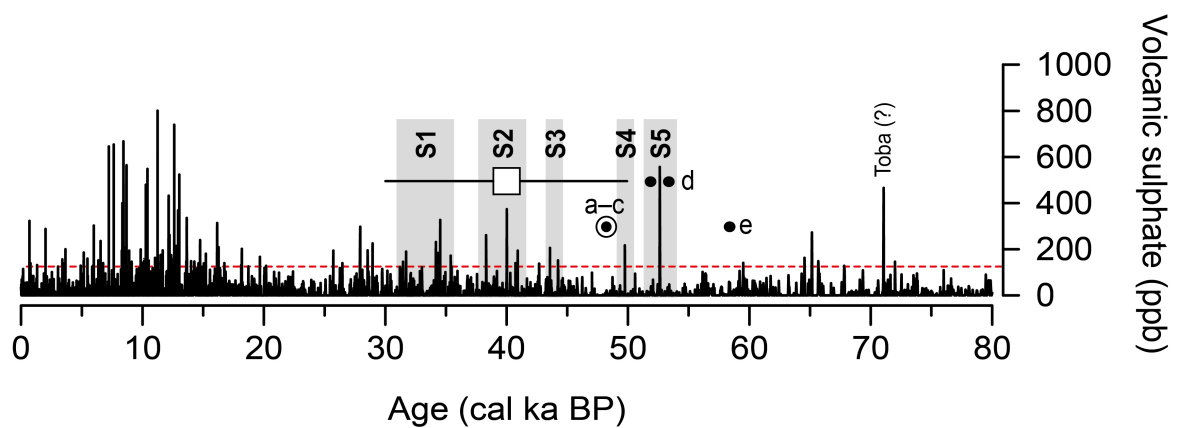


799 The c.  $40 \pm 10$  ka age estimate of the PIG7 sample is similar in magnitude to existing age  
800 estimates obtained from the Þórsmörk region. It is also a closer approximation to ‘known’  
801 ages for this deposit than, for example, the glass-phase TL age of  $23.4 \pm 2.4$  ka obtained from  
802 deposits associated with the c. 75 ka Toba eruption [124]. Post depositional thermal annealing  
803 of the PIG7 sample could have reduced its measured age, but there are no currently active  
804 thermal areas in the Þórsmörk valley. Our c.  $40 \pm 10$  ka age estimate also eliminates the  
805 possibility of a c. 200 ka eruption age for deposits at the PIG7 site. Following the SAR-TL  
806 experiments, we examined glass shards in the PIG1b and PIG7 samples for the presence of  
807 spontaneous fission-tracks. None were observed. The absence of natural fission-tracks in  
808 volcanic glass with a c. 3–4.5 ppm uranium and c. 10–14.5 ppm thorium content provides an  
809 additional age constraint of  $< c.100$  ka, and rules out the possibility of a c. 200 ka eruption age  
810 in more than one location within the Þórsmörk valley.

811

812 The  $40 \pm 10$  ka age is potentially younger than the established age of NAAZ2 and raises the  
813 intriguing possibility of multiple ignimbrite- or rhyolitic-ash forming eruptions in the area  
814 between 60–30 ka. Lacasse et al. [2, 4] first suggested the PIG is the terrestrial geochemical  
815 equivalent of North Atlantic Ash Zone 2 (NAAZ-2). NAAZ-2 was originally dated in marine cores  
816 to around 64 ka [46]. Later, correlation ages of 48.5–58 ka were proposed by comparing the  
817 astronomically calibrated oxygen isotope time scale from marine cores with the Greenland  
818 GISPII ice core incremental timescale [9, 86]. The widespread distribution of the Vedde Ash  
819 and NAAZ-II in marine cores of the North Atlantic has been linked with ice rafting [9, 46],  
820 raising doubts over the precision of c. 64–48 ka correlation ages for NAAZ-II in marine cores.  
821 The spread of ages within NAAZ-II could also indicate more than one eruption event. Zielinski  
822 et al. [9] proposed that NAAZ-II was the result of two simultaneous eruptions from Katla and

823 Torfajökull based on two distinct tephra deposits with similar chemical composition to NAAZ-  
 824 II and the PIG found in Greenland ice cores at 53.5 ka and 57.3 ka [86, 87] (Fig. 9). The c. 40  
 825 ka age estimate for the PIG7 sample is approximately 23% younger these ice core ages, but  
 826 coeval with an elevated volcanic sulphate peak in the GISP2 ice core record centred on 40 ka  
 827 (Fig. 9). Moreover, the tephrochronology of 60-30 ka eruptions from Iceland has recently  
 828 been geochemically mapped in unprecedented detail and supports the possibility of multiple  
 829 large rhyolite-forming eruptions from volcanic complexes in and around Þórsmörk during this  
 830 period.



831 □ PIG7 SAR-TL age S1–S5 Volcanic sulphate >126 ppb (99% percentile) in SAR-TL range  
 ● Closest geochemical correlation match • Geochemical correlation match

832 **Figure 9 The GISP2 Volcanic Sulphate record of palaeovolcanism for the last 80,000 years**  
 833 **compared to new SAR-TL age estimates for Þórsmörk Ignimbrite.** Notes: IC ka = ice core  
 834 years before present; References: (a) [53]; (b), (c) [2, 4]; (d) [9]; (e) [46].

835  
 836 To summarise, TL screening and dating of volcanic glass in tephra holds great potential,  
 837 particularly for the rapid classification of geochemically similar volcanic systems with widely  
 838 separated eruption events. Whether all the ignimbrite deposits in the Þórsmörk area are from  
 839 the same eruption event remains uncertain and warrants further investigation. Luminescence

840 and radiometric dating of other deposits in the Þórsmörk area is recommended to determine  
841 if more than one ignimbrite-forming eruption event occurred between 60-30 ka and further  
842 improve the tephrochronological record of Iceland.

843

#### 844 **Conclusions**

845 1) To improve the Late Pleistocene tephrochronology of Iceland, NW Europe, and the North  
846 Atlantic and Arctic regions, we investigated the thermoluminescence (TL) dose response  
847 characteristics of rhyolitic volcanic glass produced by four large Plinian eruptions from  
848 Iceland: the c. 50 ka Þórsmörk Ignimbrite, Askja 1875 AD, Öræfi 1362 AD and the Late Pliocene  
849 Óþoli Tephra,

850

851 2) Our screening experiments showed an unequivocal age-related increase in naturally  
852 retained glass-phase TL. Single aliquot regeneration-TL analysis of volcanic-glass from the  
853 Þórsmörk Ignimbrite produced an age estimate of c.  $40 \pm 10$  ka, supporting evidence for a  
854 major eruption in the Þórsmörk area of Southern Iceland 30–60 ka rather than c. 200 ka.

855

856 3) The application of combined glass-phase thermoluminescence and radiometric dating at  
857 multiple sites in the Þórsmörk area could reveal if more than one ignimbrite-forming eruption  
858 occurred between 30-60 ka. Results from the Óþoli tephra were a similar order of magnitude  
859 to its established c. 2 Ma age, but further investigation of sensitivity change and signal loss  
860 from 'older' volcanic glass deposits is required. The tephrochronological record of Iceland  
861 could be improved using TL analysis of volcanic glass deposits.

862

#### 863 **Acknowledgements**

864 SJR, AJD and DCWS undertook fieldwork funded by National Environmental Research Council  
865 (NERC) Grant no. GT 04/97/85/ES and the University of Edinburgh Moray Endowment Fund  
866 and Small Projects Grant; DCWS provided access to and support with luminescence analysis  
867 and interpretation. AJD acknowledges support of the National Science Foundation of America  
868 grant 1249313. SJR acknowledges additional support from BAS. The funders had no role in  
869 study design, data collection and analysis, decision to publish, or preparation of the  
870 manuscript. Thanks to Rob Austin-Smith, Tom Bradwell, Jeremy Everest and Bob McCulloch  
871 for their assistance in the field, John Westgate for examining Þórsmörk Ignimbrite PIG 1b and  
872 PIG7 samples for fission-tracks, Peter Hill, Paula McDade, Anthony Newton, and Shari Preece  
873 for assistance with geochemical analysis. The authors have no competing interests. Data  
874 availability: All data are available from the corresponding author ([sjro@bas.ac.uk](mailto:sjro@bas.ac.uk)) and the  
875 NERC Polar Data Centre. All necessary permits were obtained for the described study, which  
876 complied with all relevant regulations.

## 877 **References**

- 878 1. Thórarinsson S. Ignimbrít í Þórsmörk. (Ignimbrite in Þórsmörk). Náttúrufræðingurinn.  
879 1969;39:139-55.
- 880 2. Lacasse C, Sigurdsson H, Johannesson H, Paterne M, Carey S. Source of Ash-Zone-1 in  
881 the North-Atlantic. Bulletin of Volcanology. 1995;57(1):18-32.  
882 doi:10.1007/Bf00298704. PubMed PMID: WOS:A1995RB63400002.
- 883 3. Sigurdsson H, McIntosh WN, Dunbar N, Lacasse C, Carey SN. Thorsmörk ignimbrite in  
884 Iceland: possible source of North Atlantic Ash Zone 2. EOS Trans American Geophysical  
885 Union, Boston, 26-29 May 1998. 1998;EOS Trans. AGU, Spring Meet.  
886 Suppl.(79(17)):S172.
- 887 4. Lacasse C, Sigurdsson H, Carey S, Paterne M, Guichard F. North Atlantic deep-sea  
888 sedimentation of Late Quaternary tephra from the Iceland hotspot. Marine Geology.  
889 1996;129(3-4):207-35. doi:10.1016/0025-3227(96)83346-9. PubMed PMID:  
890 WOS:A1996TV77400003.
- 891 5. Blockley SPE, Bourne AJ, Brauer A, Davies SM, Hardiman M, Harding PR, et al.  
892 Tephrochronology and the extended intimate (integration of ice-core, marine and  
893 terrestrial records) event stratigraphy 8–128 ka b2k. Quaternary Science Reviews.  
894 2014;106:88-100. doi: <http://dx.doi.org/10.1016/j.quascirev.2014.11.002>.
- 895 6. Thórarinsson S. Askja on fire. Reykjavík: Almenna Bókafélagid; 1963.

- 896 7. Dugmore AJ. Tephrochronological studies of Holocene glacier fluctuations in south  
897 Iceland. In: Oerlemans J, editor. Glacier fluctuations and climatic change: Kluwer  
898 Academic Publishers; 1989. p. 37-55.
- 899 8. Zielinski GA, Germani MS, Larsen G, Baillie MGL, Whitlow S, Twickler MS, et al. Evidence  
900 of the Eldgja (Iceland) Eruption in the Gisp2 Greenland Ice Core - Relationship to  
901 Eruption Processes and Climatic Conditions in the 10th-Century. *Holocene*.  
902 1995;5(2):129-40. doi:10.1177/095968369500500201. PubMed PMID:  
903 WOS:A1995RB22100001.
- 904 9. Zielinski GA, Mayewski PA, Meeker LD, Gronvold K, Germani MS, Whitlow S, et al.  
905 Volcanic aerosol records and tephrochronology of the Summit, Greenland, ice cores.  
906 *Journal of Geophysical Research-Oceans*. 1997;102(C12):26625-40.  
907 doi:10.1029/96jc03547. PubMed PMID: WOS:A1997YJ67100027.
- 908 10. Dugmore AJ, Newton AJ, Edwards KJ, Larsen G, Blackford JJ, Cook GT. Long-distance  
909 marker horizons from small-scale eruptions: British tephra deposits from the AD 1510  
910 eruption of Hekla, Iceland. *Journal of Quaternary Science*. 1996;11(6):511-6. doi:  
911 10.1002/(Sici)1099-1417(199611/12)11:6<511::Aid-Jqs284>3.0.Co;2-C. PubMed PMID:  
912 WOS:A1996WE01200006.
- 913 11. Larsen G, Dugmore A, Newton A. Geochemistry of historical-age silicic tephtras in  
914 Iceland. *Holocene*. 1999;9(4):463-71. doi:10.1191/095968399669624108. PubMed  
915 PMID: WOS:000081526000007.
- 916 12. Wastegard S, Wohlfarth B, Subetto DA, Sapelko TV. Extending the known distribution  
917 of the Younger Dryas Vedde Ash into northwestern Russia. *Journal of Quaternary  
918 Science*. 2000;15(6):581-6. doi:10.1002/1099-1417(200009)15:6<581::Aid-  
919 Jqs558>3.3.Co;2-V. PubMed PMID: WOS:000089379900003.
- 920 13. Wastegard S, Turney CSM, Lowe JJ, Roberts SJ. New discoveries of the Vedde Ash in  
921 southern Sweden and Scotland. *Boreas*. 2000;29(1):72-8. PubMed PMID:  
922 WOS:000086023300006.
- 923 14. Wastegard S, Rasmussen TL. New tephra horizons from Oxygen Isotope Stage 5 in the  
924 North Atlantic: correlation potential for terrestrial, marine and ice-core archives. *Quat  
925 Sci Rev*. 2001;20(15):1587-93. doi:10.1016/S0277-3791(01)00055-5. PubMed PMID:  
926 WOS:000171249500002.
- 927 15. Wastegard S, Hall VA, Hannon GE, van den Bogaard C, Pilcher JR, Sigurgeirsson MA, et  
928 al. Rhyolitic tephra horizons in northwestern Europe and Iceland from the AD 700s-  
929 800s: a potential alternative for dating first human impact. *Holocene*. 2003;13(2):277-  
930 83. doi: 10.1191/0959683603hl617rr. PubMed PMID: WOS:000181279000011.
- 931 16. Wastegard S, Bjorck S, Greve C, Rasmussen TL. A tephra-based correlation between the  
932 Faroe Islands and the Norwegian Sea raises questions about chronological relationships  
933 during the last interglacial. *Terra Nova*. 2005;17(1):7-12. doi: 10.1111/j.1365-  
934 3121.2004.00578.x. PubMed PMID: WOS:000227350400002.
- 935 17. Wastegard S. Late Quaternary tephrochronology of Sweden: a review. *Quaternary  
936 International*. 2005;130:49-62. doi: 10.1016/j.quaint.2004.04.030. PubMed PMID:  
937 WOS:000226424200005.
- 938 18. Wastegard S, Rasmussen TL, Kuijpers A, Nielsen T, van Weering TCE. Composition and  
939 origin of ash zones from Marine Isotope Stages 3 and 2 in the North Atlantic. *Quat Sci  
940 Rev*. 2006;25(17-18):2409-19. doi: 10.1016/j.quascirev.2006.03.001. PubMed PMID:  
941 WOS:000240819000024.

- 942 19. Rasmussen TL, Wastegard S, Kuijpers E, van Weering TCE, Heinemeier J, Thomsen E.  
943 Stratigraphy and distribution of tephra layers in marine sediment cores from the Faeroe  
944 Islands, North Atlantic. *Marine Geology*. 2003;199(3-4):263-77. doi: 10.1016/S0025-  
945 3227(03)00219-6. PubMed PMID: WOS:000185176400004.
- 946 20. Wallrabe-Adams HJ, Lackschewitz KS. Chemical composition, distribution, and origin of  
947 silicic volcanic ash layers in the Greenland-Iceland-Norwegian Sea: explosive volcanism  
948 from 10 to 300 ka as recorded in deep-sea sediments. *Marine Geology*. 2003;193(3-  
949 4):273-93. doi: Pii S0025-3227(02)00661-8 Doi 10.1016/S0025-3227(02)00661-8.  
950 PubMed PMID: WOS:000181296600007.
- 951 21. Davies SM, Branch NP, Lowe J, Turney CSM. Towards a European tephrochronological  
952 framework for termination 1 and the early holocene. *Philosophical Transactions of the*  
953 *Royal Society of London Series a-Mathematical Physical and Engineering Sciences*.  
954 2002;360(1793):767-802. doi: 10.1098/rsta.2001.0964. PubMed PMID:  
955 ISI:000175121800010.
- 956 22. Davies SM, Wastegard S, Wohlfarth B. Extending the limits of the Borrobol Tephra to  
957 Scandinavia and detection of new early Holocene tephras. *Quaternary Research*.  
958 2003;59(3):345-52. doi: 10.1016/S0033-5894(03)00035-8. PubMed PMID:  
959 WOS:000183386500007.
- 960 23. Davies SM, Wastegard S, Rasmussen TL, Svensson A, Johnsen SJ, Steffensen JP, et al.  
961 Identification of the Fugloyarbanki tephra in the NGRIP ice core: a key tie-point for  
962 marine and ice-core sequences during the last glacial period. *Journal of Quaternary*  
963 *Science*. 2008;23(5):409-14. doi: 10.1002/jqs.1182. PubMed PMID:  
964 WOS:000257958100002.
- 965 24. Davies SM, Abbott PM, Pearce NJG, Wastegard S, Blockley SPE. Integrating the  
966 INTIMATE records using tephrochronology: rising to the challenge. *Quat Sci Rev*.  
967 2012;36:11-27. doi: 10.1016/j.quascirev.2011.04.005. PubMed PMID:  
968 WOS:000301825900003.
- 969 25. Davies SM, Abbott PM, Meara RH, Pearce NJG, Austin WEN, Chapman MR, et al. A North  
970 Atlantic tephrostratigraphical framework for 130–60 ka b2k: new tephra discoveries,  
971 marine-based correlations, and future challenges. *Quaternary Science Reviews*.  
972 2014;106:101-21. doi: <http://dx.doi.org/10.1016/j.quascirev.2014.03.024>.
- 973 26. Pyne-O'Donnell SDF. Three new distal tephras in sediments spanning the Last Glacial-  
974 Interglacial Transition in Scotland. *Journal of Quaternary Science*. 2007;22(6):559-70.  
975 doi: 10.1002/jqs.1066. PubMed PMID: WOS:000249439600001.
- 976 27. Pyne-O'Donnell SDF, Blockley SPE, Turney CSM, Lowe JJ. Distal volcanic ash layers in the  
977 Lateglacial Interstadial (GI-1): problems of stratigraphic discrimination. *Quat Sci Rev*.  
978 2008;27(1-2):72-84. doi: 10.1016/j.quascirev.2007.02.019. PubMed PMID:  
979 WOS:000254196600007.
- 980 28. Beget JE, Keskinen MJ. Trace-element geochemistry of individual glass shards of the Old  
981 Crow tephra and the age of the Delta glaciation, central Alaska. *Quaternary Research*.  
982 2003;60(1):63-9. doi: 10.1016/S0033-5894(03)00095-4. PubMed PMID:  
983 WOS:000184258400008.
- 984 29. Dugmore AJ, Larsen G, Newton AJ. 7 Tephra Isochrones in Scotland. *Holocene*.  
985 1995;5(3):257-66. doi:10.1177/095968369500500301. PubMed PMID:  
986 WOS:A1995RW28900001.
- 987 30. Pearce NJG, Alloway BV, Westgate JA. Mid-Pleistocene silicic tephra beds in the  
988 Auckland region, New Zealand: Their correlation and origins based on the trace element

- 989 analyses of single glass shards. *Quaternary International*. 2008;178:16-43. doi:  
 990 10.1016/j.quaint.2006.09.005. PubMed PMID: WOS:000255304900005.
- 991 31. Pearce NJG, Denton JS, Perkins WT, Westgate JA, Alloway BV. Correlation and  
 992 characterisation of individual glass shards from tephra deposits using trace element  
 993 laser ablation ICP-MS analyses: current status and future potential. *Journal of*  
 994 *Quaternary Science*. 2007;22(7):721-36. doi: 10.1002/jqs.1092. PubMed PMID:  
 995 WOS:000250415800007.
- 996 32. Pearce NJG, Eastwood WJ, Westgate JA, Perkins WT. Trace-element composition of  
 997 single glass shards in distal Minoan tephra from SW Turkey. *J Geol Soc*. 2002;159:545-  
 998 56. doi:10.1144/0016-764901-129. PubMed PMID: WOS:000177855400007.
- 999 33. Pearce NJG, Westgate JA, Perkins WT, Preece SJ. The application of ICP-MS methods to  
 1000 tephrochronological problems. *Applied Geochemistry*. 2004;19(3):289-322. doi:  
 1001 10.1016/S0883-2729(03)00153-7. PubMed PMID: WOS:000189101300003.
- 1002 34. Bertrand S, Castiaux J, Juvigne E. Tephrostratigraphy of the late glacial and Holocene  
 1003 sediments of Puyehue Lake (Southern Volcanic Zone, Chile, 40 degrees S). *Quaternary*  
 1004 *Research*. 2008;70(3):343-57. doi: 10.1016/j.yqres.2008.06.001. PubMed PMID:  
 1005 WOS:000260841600001.
- 1006 35. Cioni R, D'Oriano C, Bertagnini A. Fingerprinting ash deposits of small scale eruptions by  
 1007 their physical and textural features. *Journal of Volcanology and Geothermal Research*.  
 1008 2008;177(1):277-87. doi: 10.1016/j.jvolgeores.2008.06.003. PubMed PMID:  
 1009 WOS:000260986600021.
- 1010 36. Davies SM. Were there two Borrobol Tephra during the early Lateglacial period:  
 1011 implications for tephrochronology? *Quat Sci Rev*. 2004;23(5-6):581-9. doi:  
 1012 10.1016/j.quascirev.2003.11.006. PubMed PMID: ISI:000220163100004.
- 1013 37. Davies SM, Abbott PM, Meara RH, Pearce NJG, Austin WEN, Chapman MR, et al. A North  
 1014 Atlantic tephrostratigraphical framework for 130-60 ka b2k: new tephra discoveries,  
 1015 marine-based correlations, and future challenges. *Quat Sci Rev*. 2014;106:101-21. doi:  
 1016 10.1016/j.quascirev.2014.03.024. PubMed PMID: WOS:000348010900008.
- 1017 38. Hillenbrand CD, Moreton SG, Caburlotto A, Pudsey CJ, Lucchi RG, Smellie JL, et al.  
 1018 Volcanic time-markers for Marine Isotopic Stages 6 and 5 in Southern Ocean sediments  
 1019 and Antarctic ice cores: implications for tephra correlations between palaeoclimatic  
 1020 records. *Quat Sci Rev*. 2008;27(5-6):518-40. doi: 10.1016/j.quascirev.2007.11.009.  
 1021 PubMed PMID: WOS:000255351900007.
- 1022 39. Knott JR, Sarna-Wojcicki AM, Montanez IP, Wan E. Differentiating the Bishop ash bed  
 1023 and related tephra layers by elemental-based similarity coefficients of volcanic glass  
 1024 shards using solution inductively coupled plasma-mass spectrometry (S-ICP-MS).  
 1025 *Quaternary International*. 2007;166:79-86. doi: 10.1016/j.quaint.2006.12.014. PubMed  
 1026 PMID: WOS:000247166400008.
- 1027 40. Pollard AM, Blockley SPE, Lane CS. Some numerical considerations in the geochemical  
 1028 analysis of distal microtephra. *Applied Geochemistry*. 2006;21(10):1692-714. doi:  
 1029 10.1016/j.apgeochem.2006.07.007. PubMed PMID: WOS:000241641000008.
- 1030 41. Tamura I, Yamazaki H, Mizuno K. Characteristics for the recognition of Pliocene and  
 1031 early Pleistocene marker tephra in central Japan. *Quaternary International*.  
 1032 2008;178:85-99. doi: 10.1016/j.quaint.2007.04.002. PubMed PMID:  
 1033 ISI:000255304900009.
- 1034 42. Turney CSM, Blockley SPE, Lowe JJ, Wulf S, Branch NP, Mastrolorenzo G, et al.  
 1035 Geochemical characterization of Quaternary tephra from the Campanian Province,

- 1036 Italy. *Quaternary International*. 2008;178:288-305. doi: 10.1016/j.quaint.2007.02.007.  
 1037 PubMed PMID: WOS:000255304900023.
- 1038 43. Shane P, Martin SB, Smith VC, Beggs KF, Darragh MB, Cole JW, et al. Multiple rhyolite  
 1039 magmas and basalt injection in the 17.7 ka Rerewhakaaitu eruption episode from  
 1040 Tarawera volcanic complex, New Zealand. *Journal of Volcanology and Geothermal  
 1041 Research*. 2007;164(1-2):1-26. doi: 10.1016/j.jvolgeores.2007.04.003. PubMed PMID:  
 1042 WOS:000248766400001.
- 1043 44. Shane P, Nairn IA, Martin SB, Smith VC. Compositional heterogeneity in tephra deposits  
 1044 resulting from the eruption of multiple magma bodies: Implications for  
 1045 tephrochronology. *Quaternary International*. 2008;178:44-53. doi:  
 1046 10.1016/j.quaint.2006.11.014. PubMed PMID: WOS:000255304900006.
- 1047 45. Ruddiman WF, Glover LK. Ice-Rafted Volcanic Ash - a Tracer of North-Atlantic Paleo-  
 1048 Circulation. *Transactions-American Geophysical Union*. 1972;53(4):423-&. PubMed  
 1049 PMID: WOS:A1972L950100407.
- 1050 46. Ruddiman WF, Glover LK. Vertical Mixing of Ice-Rafted Volcanic Ash in North-Atlantic  
 1051 Sediments. *Geological Society of America Bulletin*. 1972;83(9):2817-&. doi: Doi  
 1052 10.1130/0016-7606(1972)83[2817:Vmoiva]2.0.Co;2. PubMed PMID:  
 1053 WOS:A1972N400300019.
- 1054 47. Pollard AM, Blockley SPE, Ward KR. Chemical alteration of tephra in the depositional  
 1055 environment: theoretical stability modelling. *Journal of Quaternary Science*.  
 1056 2003;18(5):385-94. doi: 10.1002/jqs.760. PubMed PMID: WOS:000184038700002.
- 1057 48. Blockley SPE, Pyne-O'Donnell SDF, Lowe JJ, Matthews IP, Stone A, Pollard AM, et al. A  
 1058 new and less destructive laboratory procedure for the physical separation of distal glass  
 1059 tephra shards from sediments. *Quat Sci Rev*. 2005;24(16-17):1952-60. doi:  
 1060 10.1016/j.quascirev.2004.12.008. PubMed PMID: WOS:000231044100015.
- 1061 49. Casely AF, Dugmore AJ. Climate change and 'anomalous' glacier fluctuations: the  
 1062 southwest outlets of Myrdalsjökull, Iceland. *Boreas*. 2004;33(2):108-22. doi:  
 1063 10.1080/03009480410001136. PubMed PMID: WOS:000221110900002.
- 1064 50. Dugmore AJ, Church MJ, Mairs KA, McGovern TH, Perdikaris S, Vesteinsson O.  
 1065 Abandoned farms, volcanic impacts, and woodland management: Revisiting  
 1066 pjorsardalur, the "Pompeii of Iceland". *Arctic Anthropology*. 2007;44(1):1-11. PubMed  
 1067 PMID: WOS:000248704400001.
- 1068 51. Dugmore AJ, Sugden DE. Do the anomalous fluctuations of Solheimajökull reflect ice-  
 1069 divide migration. *Boreas*. 1991;20:105-13.
- 1070 52. Edwards KJ, Dugmore AJ, Blackford JJ. Vegetational response to tephra deposition and  
 1071 land-use change in Iceland: a modern analogue and multiple working hypothesis  
 1072 approach to tephrochronology. *Polar Record*. 2004;40(213):113-20.  
 1073 doi:10.1017/S0032247403003000. PubMed PMID: WOS:000226634700003.
- 1074 53. Hafliðason H, Eiriksson J, Van Kreveld S. The tephrochronology of Iceland and the North  
 1075 Atlantic region during the Middle and Late Quaternary: a review. *Journal of Quaternary  
 1076 Science*. 2000;15(1):3-22. PubMed PMID: ISI:000085226600002.
- 1077 54. Hallsdóttir M. Pollen analytical studies of human influence on vegetation in relation to  
 1078 the Landnám tephra layer in southwest Iceland 1987. 45 p.
- 1079 55. Kirkbride MP, Dugmore AJ. Timing and significance of mid-Holocene glacier advances in  
 1080 northern and central Iceland. *Journal of Quaternary Science*. 2001;16(2):145-53.  
 1081 doi:10.1002/jqs.589. PubMed PMID: WOS:000167761700005.



- 1082 56. Kirkbride MP, Dugmore AJ. Glaciological response to distal tephra fallout from the 1947  
1083 eruption of Hekla, south Iceland. *Journal of Glaciology*. 2003;49(166):420-8.  
1084 doi:10.3189/172756503781830575. PubMed PMID: WOS:000220521200011.
- 1085 57. Kirkbride MP, Dugmore AJ. Responses of mountain lee caps in central Iceland to  
1086 Holocene climate change. *Quat Sci Rev*. 2006;25(13-14):1692-707. doi:  
1087 10.1016/j.quascirev.2005.12.004. PubMed PMID: WOS:000239940000019.
- 1088 58. Larsen G, editor Holocene volcanism in Iceland and tephrochronology as a tool in  
1089 volcanology. *Iceland 2000 – Modern Processes and Past Environments*; 2000 April 27th-  
1090 29th, 2000; Keele University, UK.
- 1091 59. Lawson IT, Gathorne-Hardy FJ, Church MJ, Newton AJ, Edwards KJ, Dugmore AJ, et al.  
1092 Environmental impacts of the Norse settlement: palaeoenvironmental data from  
1093 Myvatnssveit, northern Iceland. *Boreas*. 2007;36(1):1-19. doi:  
1094 10.1080/0300948060082798. PubMed PMID: WOS:000244148600001.
- 1095 60. Larsen C, Newton AJ, Dugmore AJ, Vilmundardottir EG. Geochemistry, dispersal,  
1096 volumes and chronology of Holocene from the Katla volcanic silicic tephra layers  
1097 system, Iceland. *Journal of Quaternary Science*. 2001;16(2):119-32. PubMed PMID:  
1098 WOS:000167761700003.
- 1099 61. Wastegard S. Early to middle Holocene silicic tephra horizons from the Katla volcanic  
1100 system, Iceland: new results from the Faroe Islands. *Journal of Quaternary Science*.  
1101 2002;17(8):723-30. doi: 10.1002/jqs.724. PubMed PMID: WOS:000180149700001.
- 1102 62. Selbekk RS, Tronnes RG. The 1362 AD Oraefajoull eruption, Iceland: Petrology and  
1103 geochemistry of large-volume homogeneous rhyolite. *Journal of Volcanology and*  
1104 *Geothermal Research*. 2007;160(1-2):42-58. doi: 10.1016/j.jvolgeores.2006.08.005.  
1105 PubMed PMID: WOS:000244215100003.
- 1106 63. Sarna-Wojcicki A. Tephrochronology. In: Stratton-Noller J, Sowers, J. M., Lettis, W. R.,  
1107 editor. *Quaternary Geochronology: Methods and Applications 2000*.
- 1108 64. Shane P. Tephrochronology: a new Zealand case study. *Earth-Science Reviews*.  
1109 2000;49(1-4):223-59. doi:10.1016/S0012-8252(99)00058-6. PubMed PMID:  
1110 WOS:000086702100005.
- 1111 65. Aitken M.J., 1985, *Thermoluminescence Dating*, Academic Press
- 1112 66a. Sanderson D, Warren SE, Hunter JR, editors. *The TL properties of archaeological glass*.  
1113 *Proceedings of 3rd Specialist seminar on TL and ESR dating*; 1983; PACT 9(II), 287-298,  
1114 ISBN 87-550-0915-8, Strasbourg
- 1115 66b. Sanderson D.C.W., 1982, *The thermoluminescence of archaeological glass*, MPhil  
1116 Thesis, University of Bradford)
- 1117 67. Ward S. *The thermoluminescence of glass slices and their potential as radiation*  
1118 *dosimeters in the 0-160 kGy range*. BSc dissertation, University of Strathclyde; 1988.
- 1119 68. Huntley DJ, Bailey DC. Obsidian Source identification by thermoluminescence.  
1120 *Archaeometry*. 1978;20(2):159-70.
- 1121 69. Westgate JA. Isothermal Plateau Fission-Track Ages of Hydrated Glass Shards from Silicic  
1122 Tephra Beds. *Earth and Planetary Science Letters*. 1989;95(3-4):226-34.  
1123 doi:10.1016/0012-821x(89)90099-X. PubMed PMID: WOS:A1989CC77700004.
- 1124 70. Westgate J, Sandhu A, Shane P. Fission-Track Dating. In: Taylor RE, Aitken MJ, editors.  
1125 *Chronometric Dating in Archaeology*. Boston, MA: Springer US; 1997. p. 127-58.
- 1126 71. Westgate JA, Preece SJ, Froese DG, Walter RC, Sandhu AS, Schweger CE. Dating early  
1127 and middle (Reid) pleistocene glaciations in central Yukon by tephrochronology.

- 1128 Quaternary Research. 2001;56(3):335-48. doi:10.1006/qres.2001.2274. PubMed PMID:  
1129 WOS:000172212000005.
- 1130 72. Bigazzi G, Laurenzi MA, Soligo M, Tuccimei P. Multi-method approach to dating glass:  
1131 The case of Basiluzzo Islet (Aeolian archipelago, Italy). Journal of Volcanology and  
1132 Geothermal Research. 2008;177(1):244-50. doi: 10.1016/j.jvolgeores.2007.10.005.  
1133 PubMed PMID: WOS:000260986600018.
- 1134 73. Berger GW. The Use of Glass for Dating Volcanic Ash by Thermoluminescence. Journal  
1135 of Geophysical Research-Solid Earth. 1991;96(B12):19705-20. doi: 10.1029/91jb01899.  
1136 PubMed PMID: WOS:A1991GQ69100013.
- 1137 74. Berger GW. Dating Volcanic Ash by Use of Thermoluminescence. Geology.  
1138 1992;20(1):11-4. doi:10.1130/0091-7613(1992)020<0011:Dvabuo>2.3.Co;2. PubMed  
1139 PMID: WOS:A1992GZ53700003.
- 1140 75. Roberts SJ, Sigurvinsson JR, Westgate JA, Sandhu A. Late Pliocene glaciation and  
1141 landscape evolution of Vestfirðir, Northwest Iceland. Quat Sci Rev. 2007;26(1-2):243-  
1142 63. doi: 10.1016/j.quascirev.2006.09.004. PubMed PMID: ISI:000244024800017.
- 1143 76. Jorgensen KA. The Thorsmork Ignimbrite - an Unusual Comenditic Pyroclastic Flow in  
1144 Southern Iceland. Journal of Volcanology and Geothermal Research. 1980;8(1):7-22.  
1145 doi:10.1016/0377-0273(80)90004-9. PubMed PMID: WOS:A1980KF92900002.
- 1146 77. Jorgensen KA. The eruption of Þórsmörk Ignimbrite, south Iceland. Reykjavik: Nordic  
1147 Volcanological Institute, Report no. 8103., 1981.
- 1148 78. McGarvie DW, editor Torfajökull – the world’s most active rhyolite volcano. Iceland  
1149 2000 – Modern Processes and Past Environments; 2000 April 27th-29th 2000; Keele  
1150 University, UK.
- 1151 79. Thórarinnsson S, Sæmundsson K. Volcanic activity in historical time. Jökull. 1979;29:29-  
1152 32.
- 1153 80. Jakobsson SP. Outline of the petrology of Iceland. Jökull. 1979;29:57-73.
- 1154 81. Jakobsson SP. Chemistry and distribution pattern of Recent basaltic rocks in Iceland.  
1155 Lithos. 1972;5:365-86.
- 1156 82. Imsland P. The Petrology of Iceland: Some General Remarks. Reykjavik: Nordic  
1157 Volcanological Institute Report 7808, pp. 2, 1978.
- 1158 83. Sæmundsson K. Outline of the Geology of Iceland. Jökull. 1979;29:7-28.
- 1159 84. Jorgensen KA. Mineralogy and Petrology of Alkaline Granophyric Xenoliths from the  
1160 Thorsmork Ignimbrite, Southern Iceland. Lithos. 1987;20(2):153-68. doi: Doi  
1161 10.1016/0024-4937(87)90004-1. PubMed PMID: WOS:A1987G439900004.
- 1162 85. Sparks RSJ, Bursik MI, Carey SN, Gilbert JS, Glaze LS, Sigurdsson H, et al. Volcanic Plumes.  
1163 Chichester: John Wiley and Sons; 1997. 574 p.
- 1164 86. Ram M, Gayley RI. Long-Range Transport of Volcanic Ash to the Greenland Ice-Sheet.  
1165 Nature. 1991;349(6308):401-4. doi:10.1038/349401a0. PubMed PMID:  
1166 WOS:A1991EV51400045.
- 1167 87. Ram M, Donarummo J, Sheridan M. Volcanic ash from Icelandic similar to 57,300 yr BP  
1168 eruption found in GISP2 (Greenland) ice core. Geophysical Research Letters.  
1169 1996;23(22):3167-9. doi:10.1029/96gl03099. PubMed PMID: WOS:A1996VQ92400025.
- 1170 88. Hafliðason H, Eiríksson J, Van Kreveld S. The tephrochronology of Iceland and the North  
1171 Atlantic region during the Middle and Late Quaternary: a review. Journal of Quaternary  
1172 Science. 2000;15(1):3-22. PubMed PMID: ISI:000085226600002.

- 1173 89. Sparks RSJ, Wilson L, Sigurdsson H. The Pyroclastic Deposits of the 1875 Eruption of  
1174 Askja, Iceland. *Philos T R Soc A*. 1981;299(1447):241-+. doi:10.1098/rsta.1981.0023.  
1175 PubMed PMID: WOS:A1981LA47100001.
- 1176 90. Sigurdsson H, Sparks RSJ. Petrology of Rhyolitic and Mixed Magma Ejecta from the 1875  
1177 Eruption of Askja, Iceland. *Journal of Petrology*. 1981;22(1):41-84. PubMed PMID:  
1178 WOS:A1981LD62800002.
- 1179 91. Macdonald R, Sparks RSJ, Sigurdsson H, Matthey DP, Mcgarvie DW, Smith RL. The 1875  
1180 Eruption of Askja Volcano, Iceland - Combined Fractional Crystallization and Selective  
1181 Contamination in the Generation of Rhyolitic Magma. *Mineralogical Magazine*.  
1182 1987;51(360):183-202. doi:10.1180/minmag.1987.051.360.01. PubMed PMID:  
1183 WOS:A1987H622300001.
- 1184 92. Mohn H. Askeregnen den 29de-30te Marts 1875. *Forhandlinger i Videnskaps-selskabet*  
1185 *i Christiania aar 1877*. 1877;10: 1–12.
- 1186 93. Einarsson T. Tephrochronology. In: Berglund BE, editor. *Handbook of Holocene*  
1187 *Palaeoecology and Palaeohydrology*: John Wiley and Sons; 1986. p. 329-42.
- 1188 94. Bergman J, Wastegard S, Hammarlund D, Wohlfarth B, Roberts SJ. Holocene tephra  
1189 horizons at Klocka Bog, west-central Sweden: aspects of reproducibility in subarctic peat  
1190 deposits. *Journal of Quaternary Science*. 2004;19(3):241-9. doi: 10.1002/jqs.833.  
1191 PubMed PMID: WOS:000221238800003.
- 1192 95. Pilcher JR, Hall VA, McCormac FG. Dates of Holocene Icelandic Volcanic-Eruptions from  
1193 Tephra Layers in Irish Peats. *Holocene*. 1995;5(1):103-10.  
1194 doi:10.1177/095968369500500111. PubMed PMID: WOS:A1995QX87900011.
- 1195 96. Thórarinsson S. The Öraefajökull eruption of 1362. *Acta Naturalia Islandica*. 1958;2(2):1-  
1196 99.
- 1197 97. Sigurvinsson JR. Weichselian glacial lake deposits in the Highlands of north-western  
1198 Iceland. *Jökull*. 1983;33:99-109.
- 1199 98. McKeever SWS. *Thermoluminescence of solids*. Cambridge: Cambridge University Press;  
1200 1985. 312 p.
- 1201 99. Wintle AG. *Luminescence dating: Laboratory procedures and protocols*. Radiation  
1202 *Measurements*. 1997;27(5-6):769-817. doi:10.1016/S1350-4487(97)00220-5. PubMed  
1203 PMID: WOS:000072413000007.
- 1204 100. Aitken MJ. *An introduction to optical dating. The Dating of Quaternary Sediments by*  
1205 *the Use of Photon-stimulated Luminescence*. Oxford: Oxford University Press; 1998. 270  
1206 p.
- 1207 101. Zander A, Duller GAT, Wintle AG. Multiple and single aliquot luminescence dating  
1208 techniques applied to quartz extracted from Middle and Upper Weichselian loess,  
1209 Zemechy, Czech Republic. *Journal of Quaternary Science*. 2000;15(1):51-60.  
1210 doi:10.1002/(Sici)1099-1417(200001)15:1<51::Aid-Jqs468>3.0.Co;2-6. PubMed PMID:  
1211 WOS:000085226600005.
- 1212 102. Turney CSM, Harkness DD, Lowe JJ. The use of microtephra horizons to correlate Late-  
1213 glacial lake sediment successions in Scotland. *Journal of Quaternary Science*.  
1214 1997;12(6):525-31. doi:10.1002/(Sici)1099-1417(199711/12)12:6<525::Aid-  
1215 Jqs347>3.3.Co;2-D. PubMed PMID: WOS:000071733500007.
- 1216 103. Murray AS, Wintle AG. Luminescence dating of quartz using an improved single-aliquot  
1217 regenerative-dose protocol. *Radiation Measurements*. 2000;32(1):57-73. doi:  
1218 10.1016/S1350-4487(99)00253-X. PubMed PMID: WOS:000084790600008.

- 1219 104. Murray AS, Wintle AG. The single aliquot regenerative dose protocol: potential for  
1220 improvements in reliability. *Radiation Measurements*. 2003;37(4-5):377-81. doi:  
1221 10.1016/S1350-4487(03)00053-2. PubMed PMID: WOS:000184110400015.
- 1222 105. Pawley SM, Bailey RM, Rose J, Moorlock BSP, Hamblin RJO, Booth SJ, et al. Age limits on  
1223 Middle Pleistocene glacial sediments from OSL dating, north Norfolk, UK. *Quat Sci Rev*.  
1224 2008;27(13-14):1363-77. doi: 10.1016/j.quascirev.2008.02.013. PubMed PMID:  
1225 WOS:000257604000006.
- 1226 106. Zimmerman DW. Thermoluminescent Dating Using Fine Grains from Pottery.  
1227 *Archaeometry*. 1971;13(Feb):29-52. doi: DOI 10.1111/j.1475-4754.1971.tb00028.x.  
1228 PubMed PMID: WOS:A1971Y040400005.
- 1229 107. Bell WT. Alpha dose attenuation in quartz grains for thermoluminescence dating.  
1230 *Ancient TL*. 1980;12:4-8.
- 1231 108. Mejdahl V. Thermoluminescence Dating - Beta-Dose Attenuation in Quartz Grains.  
1232 *Archaeometry*. 1979;21(Feb):61-72. doi: DOI 10.1111/j.1475-4754.1979.tb00241.x.  
1233 PubMed PMID: WOS:A1979GM02300005.
- 1234 109. Nambi KSV, Aitken MJ. Annual Dose Conversion Factors for TL-and-ESR Dating.  
1235 *Archaeometry*. 1986;28:202-5. doi:10.1111/j.1475-4754.1986.tb00388.x. PubMed  
1236 PMID: WOS:A1986D630100007.
- 1237 110. Wintle AG. Detailed Study of a Thermoluminescent Mineral Exhibiting Anomalous  
1238 Fading. *Journal of Luminescence*. 1977;15(4):385-93. doi:10.1016/0022-  
1239 2313(77)90037-0. PubMed PMID: WOS:A1977EB75500002.
- 1240 111. Sanderson DCW. Thermoluminescence dating of Scottish vitrified forts: Paisley College  
1241 of Technology; 1986 uk.bl.ethos.376105
- 1242 112. Toyoda S, Tsukamoto S, Hameaua S, Usui H, Suzuki T. Dating of Japanese Quaternary  
1243 tephra by ESR and luminescence methods. *Quaternary Geochronology*. 2006;1(4):320-  
1244 6. doi: 10.1016/j.quageo.2006.03.007. PubMed PMID: WOS:000247209900010.
- 1245 113. Auclair M, Lamothe M, Lagroix F, Banerjee SK. Luminescence investigation of loess and  
1246 tephra from halfway house section, central Alaska. *Quaternary Geochronology*.  
1247 2007;2(1-4):34-8. doi: 10.1016/j.quageo.2006.05.009. PubMed PMID:  
1248 WOS:000247210000008.
- 1249 114. Tsukamoto S, Murray AS, Huot S, Watanuki T, Denby PM, Botter-Jensen L.  
1250 Luminescence property of volcanic quartz and the use of red isothermal TL for dating  
1251 tephra. *Radiation Measurements*. 2007;42(2):190-7. doi:  
1252 10.1016/j.radmeas.2006.07.008. PubMed PMID: WOS:000247516300010.
- 1253
- 1254 115. Tsukamoto S. Luminescence, Volcanic Rocks. In: Rink JW, Thompson J, editors.  
1255 *Encyclopedia of Scientific Dating Methods*. Dordrecht: Springer Netherlands; 2013. p. 1-  
1256 5.
- 1257 116. Sanderson DCW. Fading of Thermo-Luminescence in Feldspars - Characteristics and  
1258 Corrections. *Nuclear Tracks and Radiation Measurements*. 1988;14(1-2):155-61.  
1259 PubMed PMID: WOS:A1988P853300023.
- 1260 117. Visocekas R. La luminescence de la calcite après irradiation cathodique:  
1261 thermoluminescence et luminescence par effet tunnel. France: Université de Pierre et  
1262 Marie Curie; 1979.
- 1263 118. Lamothe M, Auclair M. A solution to anomalous fading and age shortfalls in optical  
1264 dating of feldspar minerals. *Earth and Planetary Science Letters*. 1999;171(3):319-23.  
1265 doi: 10.1016/S0012-821x(99)00180-6. PubMed PMID: WOS:000082374200001.

- 1266 119. Templer RH. The Localised Transition Model of Anomalous Fading. 1986. p. 493-7.
- 1267 120. Morthekai P, Jain M, Murray AS, Thomsen KJ, Botter-Jensen L. Fading characteristics of  
1268 martian analogue materials and the applicability of a correction procedure. *Radiation*  
1269 *Measurements*. 2008;43(2-6):672-8. doi: 10.1016/j.radmeas.2008.02.019. PubMed  
1270 PMID: WOS:000257808000117.
- 1271 121. Chawla S, Rao TKG, Singhvi AK. Quartz thermoluminescence: Dose and dose-rate effects  
1272 and their implications. *Radiation Measurements*. 1998;29(1):53-63. doi:  
1273 10.1016/S1350-4487(97)00200-X. PubMed PMID: WOS:000072761500007.
- 1274 122. Bell WT. Attenuation factors for the absorbed radiation dose in quartz grains for  
1275 luminescence dating. *Ancient TL*. 1979;8:2-13.
- 1276 123. Bell WT. TL dating: radiation dose rate data. *Archaeometry*. 1979;21:243.
- 1277 124. Horn P, Müller-Sohnius D, Storzer D, Zöller L. K-Ar-, fission-track-, and thermolumines-  
1278 cence ages of Quaternary volcanic tuffs and their bearing on Acheulian artifacts from  
1279 Bori, Kukdi Valley, Pune District, India. *Zeitschrift der Deutschen geologischen*  
1280 *Gesellschaft*. 1993;144:326-9.
- 1281 125. Wolfe CJ, Bjarnason IT, VanDecar JC, Solomon SC. Seismic structure of the Iceland  
1282 mantle plume. *Nature*. 1997;385(6613):245-7. doi:10.1038/385245a0. PubMed PMID:  
1283 WOS:A1997WC71100044.
- 1284 126. LeMaitre RW, Bateman P, Dudek A, Keller J, Lameyre Le Bas MJ, Sabine PA, et al. A  
1285 classification of igneous rocks and glossary of terms. Oxford: Blackwell; 1989.
- 1286 127. Rickwood PC. Boundary Lines within Petrologic Diagrams Which Use Oxides of Major  
1287 and Minor Elements. *Lithos*. 1989;22(4):247-63. doi:10.1016/0024-4937(89)90028-5.  
1288 PubMed PMID: WOS:A1989U514400001.
- 1289 128. Oskarsson N, Steinthorsson S, Sigvaldason GE. Iceland Geochemical Anomaly - Origin,  
1290 Volcanotectonics, Chemical Fractionation and Isotope Evolution of the Crust. *J Geophys*  
1291 *Res-Solid*. 1985;90(Nb12):11-25. doi:10.1029/JB090iB12p10011. PubMed PMID:  
1292 WOS:A1985ASE4800005.
- 1293 129. Sweatman TR, Long JVP. Quantitative electron microprobe analysis of rock forming  
1294 minerals. *Journal of Petrology*. 1969;7:332-79.
- 1295 130. Prescott JR, Hutton JT. Cosmic ray contributions to dose rates for luminescence and ESR  
1296 dating: large depths and long-term time variations. *Radiation Measurements*.  
1297 1994;23(497-500).
- 1298 131. Norrish K, Hutton JT. An accurate X-ray spectrographic method for the analysis of a wide  
1299 range of geological samples. *Geochimica et Cosmochimica Acta*. 1969;33:431-53.
- 1300 132. Aitken MJ, Bowman SGE. Thermoluminescence dating: assessment of alpha particle  
1301 contribution. *Archaeometry*. 1975;17:132-8.
- 1302 133. Berger GW. Progress in luminescence dating methods for Quaternary sediments. In:  
1303 Rutter NW, Catto NR, editors. *Dating Methods for Quaternary Deposits: Geological*  
1304 *Association of Canada*; 1995. p. 81-104.
- 1305